NASA Technical Memorandum 88284

Predicted Pitching Moment Characteristics of X-29A Aircraft

Gerald D. Budd

March 1987

National Aeronautics and
Space Administration

NASA Technical Memorandum 88284

Predicted Pitching Moment Characteristics of X29A Aircraft

Gerald D. Budd
Ames Research Center, Dryden Flight Research Facility, Edwards, California

1987

National Aeronautics and
Space Administration
Ames Research Center
Dryden Flight Research Facility
Edwards, California 93523-5000

SUMMARY

The predicted pitching moment characteristics of the X-29A aircraft are presented for angles of attack from 0 to 20° and Mach numbers of 0.2, 0.6, 0.9, 1.2, and 1.5 for altitudes of sea level, 4572 m (15,000 ft), 9144 m (30,000 ft), and 12,192 m (40,000 ft). These data are for both rigid and flexible aircraft and for the full range of control-surface positions. The characteristics were extracted from a nonlinear, symmetric, flexibilized wind tunnel data base.

INTRODUCTION

The X-29A is a single-seat fighter-type research aircraft powered by a single General Electric F404-GE-400 engine and is designed to fly to supersonic speeds. The X-29A was constructed with parts from many existing aircraft in an effort to reduce cost. An F-5A forward fuselage, an F-16 main landing gear, and F-16 flight control actuators were incorporated into the X-29A aircraft.

The X-29A aircraft is a radical design that incorporates several emerging and unproven technologies. Thick composite wing covers on a thin supercritical forward-swept wing with aeroelastic tailoring are used to control structural divergence. The aircraft is approximately 35 percent statically unstable longitudinally and is controllable by a digital fly-by-wire flight control system.

The predicted pitching moment characteristics of the X-29A aircraft are presented for angles of attack from 0 to 20°, and Mach numbers of 0.2 at sea level, 0.6 at 4572 m (15,000 ft), 0.9 and 1.2 at 9144 m (30,000 ft), and 1.5 at 12,192 m (40,000 ft). These data are for both rigid and flexible aircraft over the full range of control-surface positions. The characteristics were extracted from a nonlinear, symmetric, flexibilized wind tunnel data base given in reference 1. The original wind tunnel data may be found in reference 2.

A brief description of the aircraft is presented in the appendix. An overview of the X-29A flight research program is given in reference 3.

This report presents the flexible and rigid pitching moment characteristics of the X-29A aircraft and is a summary update of reference 4. It is an important source of information due to the highly statically unstable configuration of the aircraft.

NOMENCLATURE

CL	lift coefficient
CM	pitching moment coefficient
CM-DF F/R	flexible/rigid ratio of the pitching moment due to wing flap deflection
DC	canard position, trailing-edge down, positive, deg

DF wing flap position, trailing-edge down, positive, deg

DS strake flap position, trailing-edge down, positive, deg

H pressure altitude, m (ft)

DISCUSSION AND RESULTS

The predicted pitching moment characteristics presented were calculated for a center-of-gravity position of fuselage station 11.46 m (451.0 in), waterline 1.64 m (64.6 in). The angle of attack was varied from 0° to 20° in 4° increments to attain the desired variation in lift coefficient. Lateral control surface positions and sideslip angle were zero. The data were calculated for both flexible and rigid aircraft (figs. 1 to 10).

Mach Effects

At lower Mach numbers, the aircraft displays a high degree of static pitch instability, nominally 35 percent. At supersonic speeds, the aerodynamic center moves aft until the aircraft becomes statically stable near Mach 1.5. This is because the aircraft center of pressure shifts with increasing Mach, which results in increased static pitch stability.

Above Mach 1.3, the aerodynamic data base is linearly extrapolated from wind tunnel data.

Flexibility Effects

Flexibility effects are known to be a function of dynamic pressure and angle of attack. Rigid data presented are referenced to zero dynamic pressure. There appears to be a reduction in lift coefficient due to flexibility at low altitudes and Mach numbers, and an increase at higher altitudes and Mach numbers. There is a slight overall increase in pitching moment. From the specific altitudes and Mach numbers, dynamic pressure effects can be inferred. There is a slight overall increase (destabilizing) in pitching moment coefficient due to flexibility. These characteristics are shown by a slight increase in pitching moment, with a small reduction in lift.

Canard Control Effectiveness

Figures 1(a) to 2(e) show the effect of canard position with varying lift coefficient (angle of attack) on the predicted flexible and rigid longitudinal static stability.

In figure 1(a), canard flow separation is seen as a reduction in canard pitching moment contribution at low altitude and at Mach 0.2. This occurs when the canard

local angle of attack (excluding upwash effects) is in excess of 20° and less than -30°. The net effect is that the aircraft approaches neutral static stability at these conditions. As shown in figures 1(b) and 1(c), canard separation occurs at reduced local angles of attack as Mach number increases to 0.6 and 0.9. This effect is characteristic of thin, sharp leading-edge, low aspect-ratio airfoils (similar to an F-104 wing). Loss of lift and canard control effectiveness is attributed to canard flow separation occurring at relatively low local angles of attack, which in turn causes a net increase in static pitch stability.

As shown in figure 2(c), flexible and rigid canard effectiveness is constant at Mach 0.9 for negative canard deflections beginning at -30° due to a constant flexible canard increment below Mach 1.05. This results in identical data for the -30° and -60° canard deflections. Because of a linear flexible canard increment beginning at Mach 1.05, rigid canard effectiveness is constant at Mach 1.2 for negative canard deflections beginning at -20° and positive deflections beginning at 10°. As shown in figure 2(d), this results in identical data for the -20°, -30°, and -60° canard deflections and identical data for the 10 and 30° canard deflections. Comparisons of figures 1 and 2 show little flexibility effect on canard control effectiveness.

Flap Control Effectiveness

Figures 3(a) to 8(e) show the effect of flap position with varying lift coefficient (angle of attack), at 20°, 0°, and -20° canard deflection, on the predicted flexible and rigid longitudinal static stability.

Flap control effectiveness is a function of flap deflection and angle of attack. A slight reduction in the lift coefficient and pitching moment contribution with positive flap deflection is seen at lower angles of attack. At higher angles of attack, there is a greater reduction in flap control effectiveness. The pitching moment producing capability of the flap is approximately 50 percent of the canard capability.

Variation in flap position has an effect on static pitch stability at higher angles of attack. An apparent increase in upwash with positive flap deflection at Mach 0.6 and 0.9 enhances canard flow separation, thereby increasing static stability. A reduction in the canard local angle of attack delays the flap-induced canard flow separation.

Flexibility effects are known to be a function of dynamic pressure and flap deflection. Comparisons of the rigid and flexible coefficients illustrate the small effect of flexibility on flap effectiveness at low altitude and Mach number conditions corresponding to low dynamic pressure. At higher Mach number conditions (higher corresponding dynamic pressures), flexibility effects become stronger except at higher flap deflections where the effects are not modeled. As shown in figure 11, this causes a reduction in flap control effectiveness.

Strake Control Effectiveness

Figures 9(a) to 10(e) show the effect of strake position with varying lift coefficient (angle of attack) on the predicted flexible and rigid longitudinal static

stability. The strake pitch control effectiveness is less than the canard or the flap, but it appears to be very nearly linear to 20° angle of attack with little variation due to flexibility. Variation in strake position seems to have minimal effect on static pitch stability.

CONCLUDING REMARKS

At low Mach numbers, the aircraft is approximately 35 percent statically unstable. The aircraft becomes slightly stable near Mach 1.5. This is because the aircraft center of pressure shifts aft with increasing Mach, which results in increased static pitch stability.

Flexibility effects were inferred to be a function of dynamic pressure and angle of attack. These characteristics are shown by a slight increase in pitching moment, with a small reduction in lift. Canard and strake control-surface effectiveness does not appear to be sensitive to flexibility, but flap effectiveness is reduced slightly.

The canard is the most powerful pitch control surface with almost twice the pitching moment producing capability of the flap. The strake is the least effective pitch control surface but maintains a nearly linear control effectiveness beyond 20° angle of attack. The flap is the most effective lifting surface, followed by the canard and the strake.

The canard is sensitive to changes in local angle of attack due to the thin surface and the sharp leading edge combined with a low aspect ratio. Loss of lift and canard control effectiveness is attributed to canard flow separation that occurs at relatively low local angles of attack causing a net increase in static pitch stability.

Static pitch stability appears to be a function of flap position at higher angles of attack. This may be due to a flap-induced canard stall or a canard-influenced wingtip stall. Reducing the canard local angle of attack tends to delay the change in pitch stability.

National Aeronautics and Space Administration
Ames Research Center
Dryden light esearch Facility
Edwards, California, October 22, 1986

APPENDIX — AIRCRAFT DESCRIPTION

The X-29A is a single-seat fighter-type aircraft (figs. 12 and 13) with a closely coupled canard immediately ahead of a thin supercritical forward-swept wing. The wing leading edge is fixed, with full-span variable camber trailing-edge flaperons (fig. 14) to maximize the lift/drag ratio and to provide lateral control. An aft-body strake flap provides the aircraft with three-surface longitudinal control. Additional physical characteristics are presented in table 1.

REFERENCES

1. Davis, J.C.; and Pearce, R.A.: X-29 Automatic Camber Control (ACC) Trim Points & Resulting Stability & Control Derivatives. 712/ENG-RPT-85-002, Grumman Aerospace Corp., 1985.

2. Charletta, R.: Series I Transonic/Supersonic Testing on a 12.5% Scale Grumman Design 712, X-29A Forward-Swept Wing Demonstrator Aircraft Model in the NASA-ARC 11 Foot and 9x7 Foot Wind Tunnels at Moffett Field, Ca. AER/T-Ames-538-1-11-97, vols. 1 to 3, Grumman Aerospace Corp., 1982.

3. Putnam, Terrill W.: X-29 Flight-Research Program. NASA TM-86025, 1984.

4. Budd, Gerald D.: Locally Linearized Longitudinal and Lateral-Directional Aerodynamic Stability and Control Derivatives for the X-29A Aircraft. NASA TM-84919, 1984.

TABLE 1. — AIRCRAFT GEOMETRY AND MASS CHARACTERISTICS

Total height, m (ft)	4.36 (14.29)
Total length, m (ft)	14.67 (48.1)
Wing	
Reference planform area, m^2 (ft^2)	17.187 (185.0)
Reference span, m (ft)	8.29 (27.2)
Reference chord, m (ft)	2.2 (7.216)
Root chord, m (ft)	2.96 (9.72)
Aspect ratio	4.0
Taper ratio	0.4
Airfoil	GAC K-Mod2 supercritical
Airfoil thickness, root, percent	6.7
Airfoil thickness, tip, percent	4.9
Dihedral angle, deg	0
Twist, deg	7
Root incidence angle, deg	-5
Quarter-chord sweep angle, deg	-33.73
Leading-edge sweep angle, deg	-29.27
Vertical tail	
Area, m^2 (ft^2)	3.14 (33.75)
Span, m (ft)	1.68 (5.5)
Chord, m (ft)	2.03 (6.67)
Root chord, m (ft)	2.36 (7.75)
Aspect ratio	2.64
Taper ratio	0.306
Airfoil	Symmetrical
Airfoil thickness, root, percent	4.0
Airfoil thickness, root, percent	4.0
Quarter-chord sweep angle, deg	41.05
Leading-edge sweep angle, deg	47.00
Canard	
Planform area, m^2 (ft^2)	11.28 (37.0)
Span, m (ft)	4.15 (13.63)
Chord, m (ft)	1.66 (5.46)
Root chord, m (ft)	2.32 (7.61)
Aspect ratio	1.47
Taper ratio	0.318
Airfoil	Symmetrical
Airfoil thickness, root, percent	5.0
Airfoil thickness, tip, percent	3.5
Dihedral angle, deg	0
Quarter-chord sweep angle, deg	23.08
Leading-edge sweep angle, deg	42.00
Deflection range, deg	+30 to -60

TABLE 1. — (Concluded)

Wing flap	
Hinge line, percent of wing root chord	0.75
Half-span, m (ft)	2.85 (9.35)
Area, m^2 (ft^2)	1.33 (14.32)
Root station, percent of wing half-span	0.28
Root chord, m (ft)	0.74 (2.43)
Hinge-line sweep angle, deg	42.0
Deflection range, deg	-10 to +25
Strake flap	
Half-span, m (ft)	0.64 (2.08)
Area, m^2(ft^2)	0.48 (5.21)
Root station, percent of strake half-span	0
Root chord, m (ft)	0.76 (2.50)
Hinge-line sweep angle, deg	0
Deflection range, deg	±30
Rudder	
Hinge line, percent of vertical stabilizer chord	0.70
Span, m (ft)	2.03 (6.67)
Area, m^2(ft^2)	0.68 (7.31)
Root station, percent of vertical stabilizer	0.18
Root chord, m (ft)	0.71 (2.33)
Hinge-line sweep angle, deg	27
Deflection range, deg	±30
Masses	
Empty weight, N (lb)	62,495 (13,948)
Useful load, N (lb)	17,310 (3882)
Fuel load, N (lb)	16,329 (3662)
Gross weight, N (lb)	79,505 (17,830)
Powerplant	
Engine	Single General Electric F404-GE-400
Sea-level static thrust, N (lb)	71,400 (16,012)

FIGURES

Figure	Description
1	CM as a function of CL; flexible, varying DC.
	(a) Mach = 0.2, H = sea level, DF = 0, DS = 0.
	(b) Mach = 0.6, H = 4572 m (15,000 ft), DF = 0, DS = 0.
	(c) Mach = 0.9, H = 9144 m (30,000 ft), DF = 0, DS = 0.
	(d) Mach = 1.2, H = 9144 m (30,000 ft), DF = 0, DS = 0.
	(e) Mach = 1.5, H = 12,192 m (40,000 ft), DF = 0, DS = 0.
2	CM as a function of CL; rigid, varying DC.
	(a) Mach = 0.2, DF = 0, DS = 0.
	(b) Mach = 0.6, DF = 0, DS = 0.
	(c) Mach = 0.9, DF = 0, DS = 0.
	(d) Mach = 1.2, DF = 0, DS = 0.
	(e) Mach = 1.5, DF = 0, DS = 0.
3	CM as a function of CL; flexible, varying DF.
	(a) Mach = 0.2, H = sea level, DC = 20, DS = 0.
	(b) Mach = 0.6, H = 4572 m (15,000 ft), DC = 20, DS = 0.
	(c) Mach = 0.9, H = 9144 m (30,000 ft), DC = 20, DS = 0.
	(d) Mach = 1.2, H = 9144 m (30,000 ft), DC = 20, DS = 0.
	(e) Mach = 1.5, H = 12,192 m (40,000 ft), DC = 20, DS = 0.
4	CM as a function of CL; rigid, varying DF.
	(a) Mach = 0.2, DC = 20, DS = 0.
	(b) Mach = 0.6, DC = 20, DS = 0.
	(c) Mach = 0.9, DC = 20, DS = 0.
	(d) Mach = 1.2, DC = 20, DS = 0.
	(e) Mach = 1.5, DC = 20, DS = 0.

Figure	Description
5	CM as a function of CL; flexible, varying DF.
	(a) Mach = 0.2, H = sea level, DC = 0, DS = 0.
	(b) Mach = 0.6, H = 4572 m (15,000 ft), DC = 0, DS = 0.
	(c) Mach = 0.9, H = 9144 m (30,000 ft), DC = 0, DS = 0.
	(d) Mach = 1.2, H = 9144 m (30,000 ft), DC = 0, DS = 0.
	(e) Mach = 1.5, H = 12,192 m (40,000 ft), DC = 0, DS = 0.
6	CM as a function of CL; rigid, varying DF.
	(a) Mach = 0.2, DC = 0, DS = 0.
	(b) Mach = 0.6, DC = 0, DS = 0.
	(c) Mach = 0.9, DC = 0, DS = 0.
	(d) Mach = 1.2, DC = 0, DS = 0.
	(e) Mach = 1.5, DC = 0, DS = 0.
7	CM as a function of CL; flexible, varying DF.
	(a) Mach = 0.2, H = sea level, DC = -20, DS = 0.
	(b) Mach = 0.6, H = 4572 m (15,000 ft), DC = -20, DS = 0.
	(c) Mach = 0.9, H = 9144 m (30,000 ft), DC = -20, DS = 0.
	(d) Mach = 1.2, H = 9144 m (30,000 ft), DC = -20, DS = 0.
	(e) Mach = 1.5, H = 12,192 m (40,000 ft), DC = -20, DS = 0.
8	CM as a function of CL; rigid, varying DF.
	(a) Mach = 0.2, DC = -20, DS = 0.
	(b) Mach = 0.6, DC = -20, DS = 0.
	(c) Mach = 0.9, DC = -20, DS = 0.
	(d) Mach = 1.2, DC = -20, DS = 0.
	(e) Mach = 1.5, DC = -20, DS = 0.

Figure	Description
9	CM as a function of CL; flexible, varying DS.
	(a) Mach = 0.2, H = sea level, DC = 0, DF = 0.
	(b) Mach = 0.6, H = 4572 m (15,000 ft), DC = 0, DF = 0.
	(c) Mach = 0.9, H = 9144 m (30,000 ft), DC = 0, DF = 0.
	(d) Mach = 1.2, H = 9144 m (30,000 ft), DC = 0, DF = 0.
	(e) Mach = 1.5, H = 12,192 m (40,000 ft), DC = 0, DF = 0.
10	CM as a function of CL; rigid, varying DS.
	(a) Mach = 0.2, DC = 0, DF = 0.
	(b) Mach = 0.6, DC = 0, DF = 0.
	(c) Mach = 0.9, DC = 0, DF = 0.
	(d) Mach = 1.2, DC = 0, DF = 0.
	(e) Mach = 1.5, DC = 0, DF = 0.
11	Wing flap pitch control flexible/rigid ratio.
12	X-29A aircraft.
13	General configuration of X-29A aircraft.
14	X-29A full-span flap geometry.

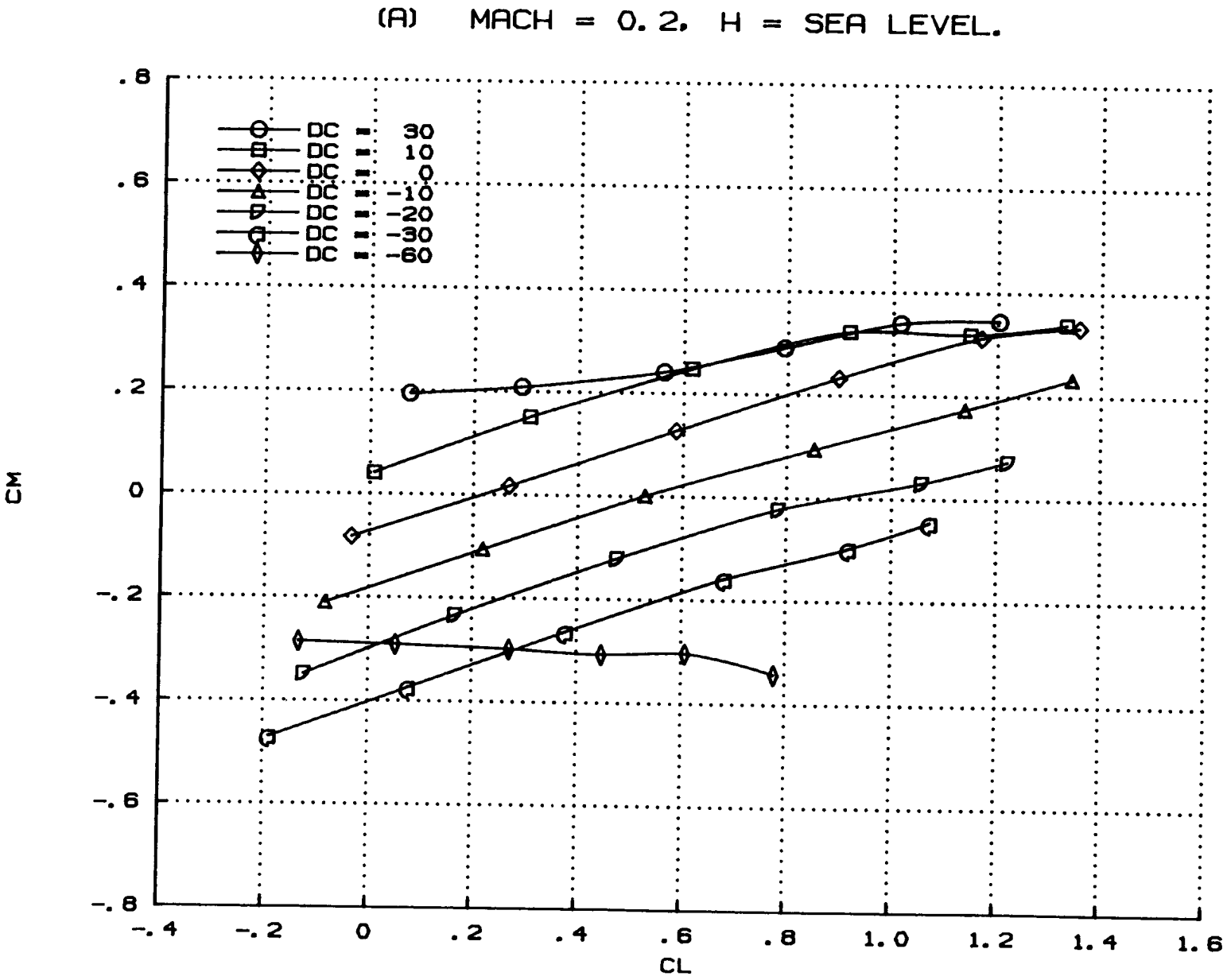

FIGURE 1. CM AS A FUNCTION OF CL. FLEXIBLE, VARYING DC.

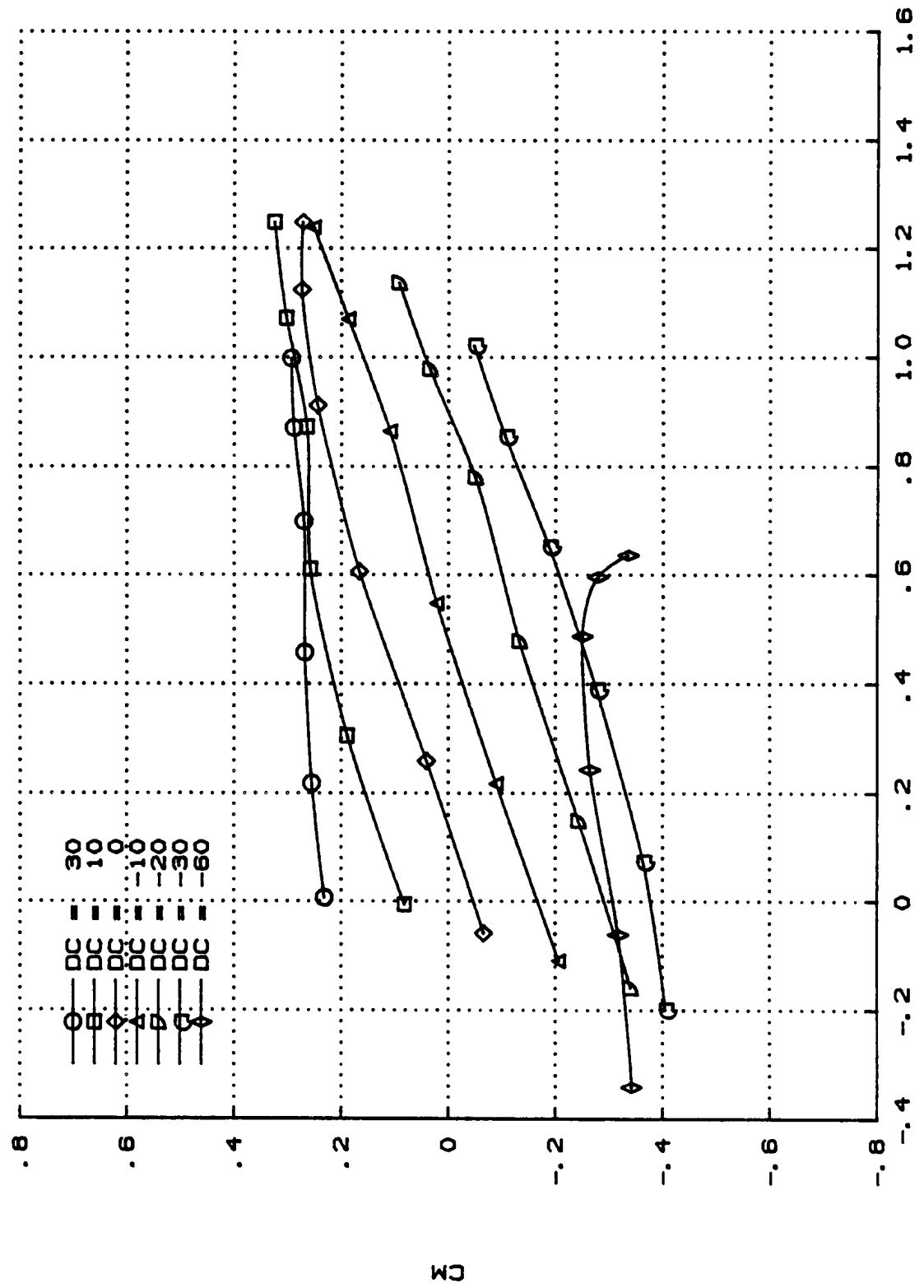

FIGURE 1. CM AS A FUNCTION OF CL, FLEXIBLE, VARYING DC.

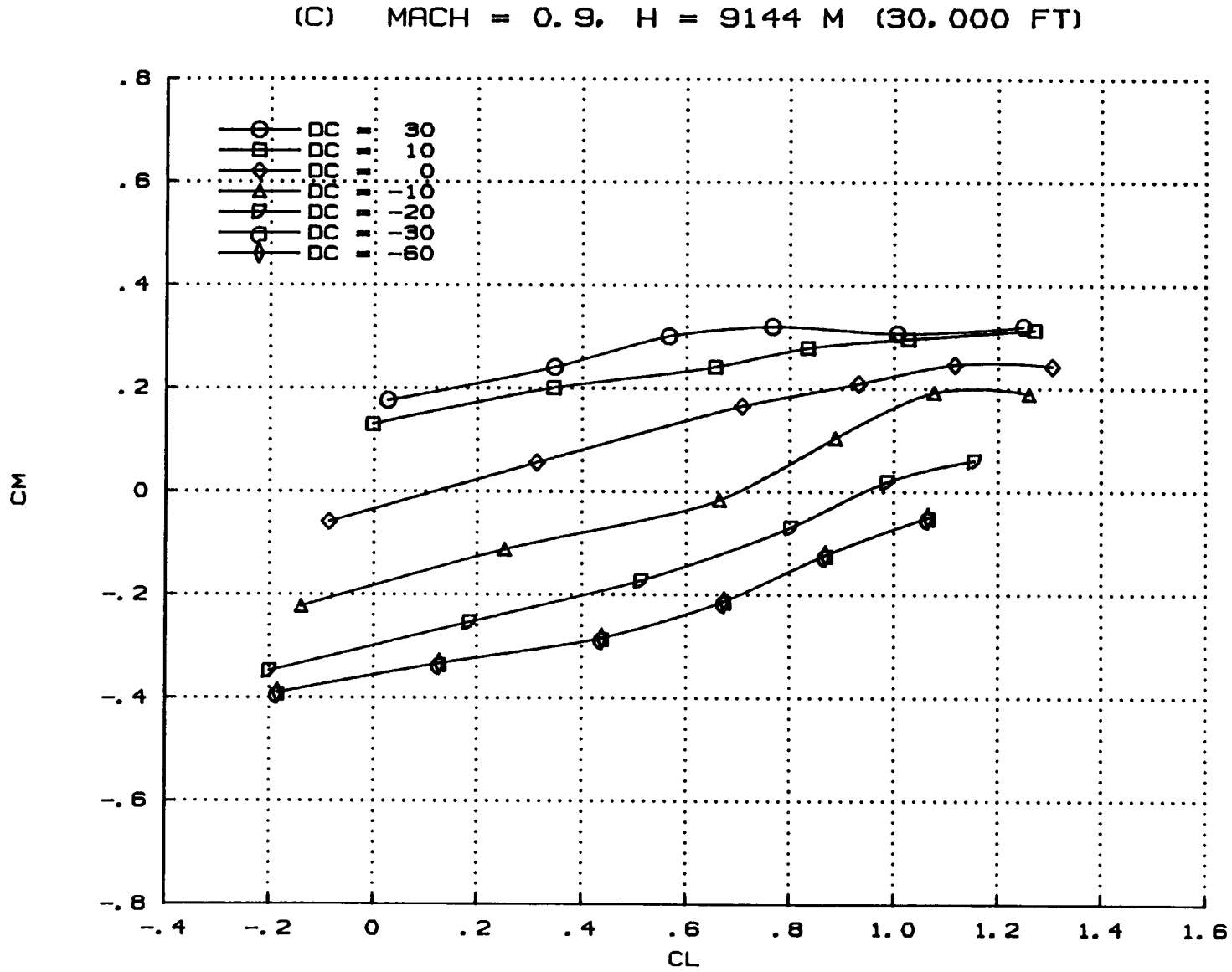

FIGURE 1. CM AS A FUNCTION OF CL. FLEXIBLE, VARYING DC.

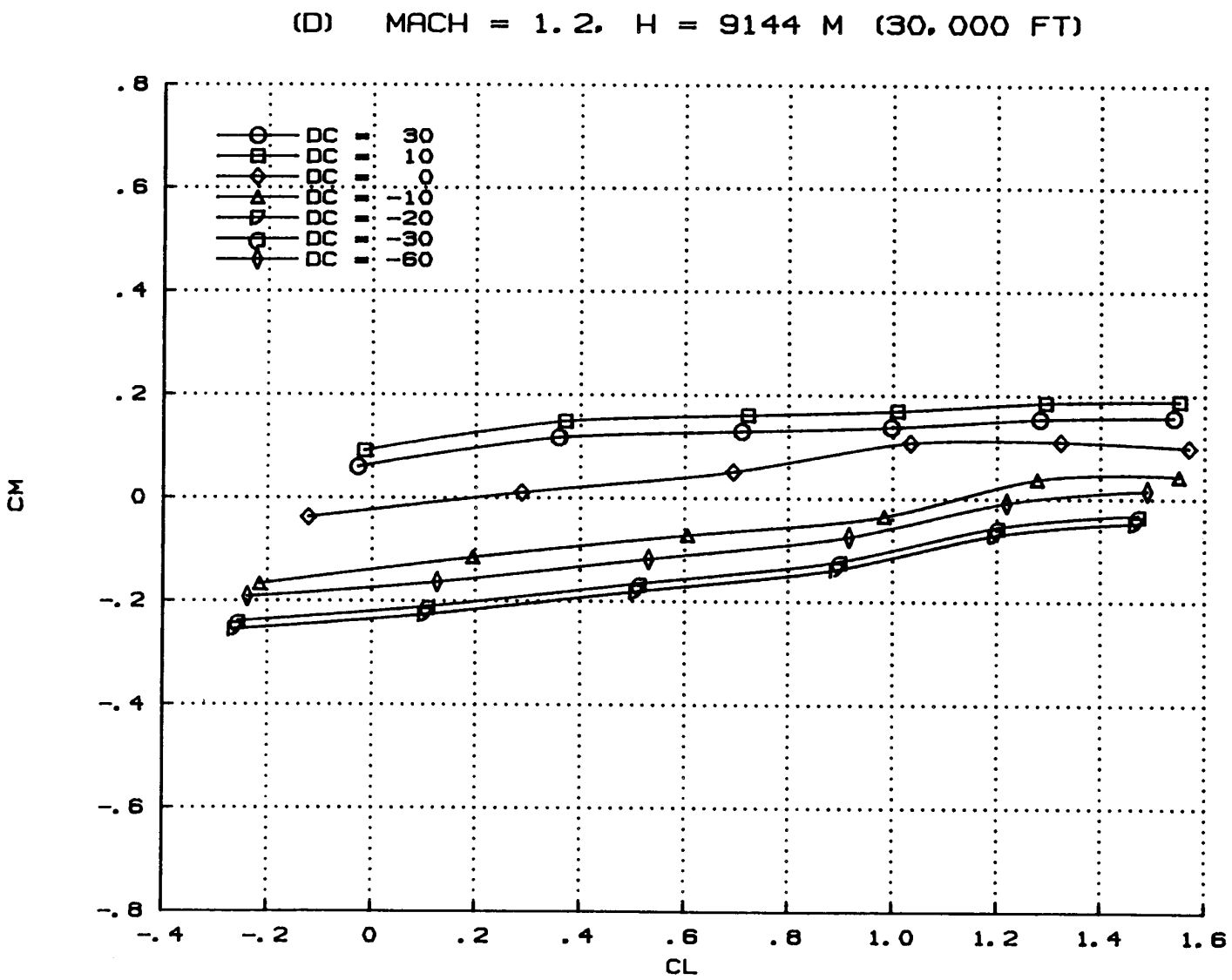

FIGURE 1. CM AS A FUNCTION OF CL. FLEXIBLE. VARYING DC.

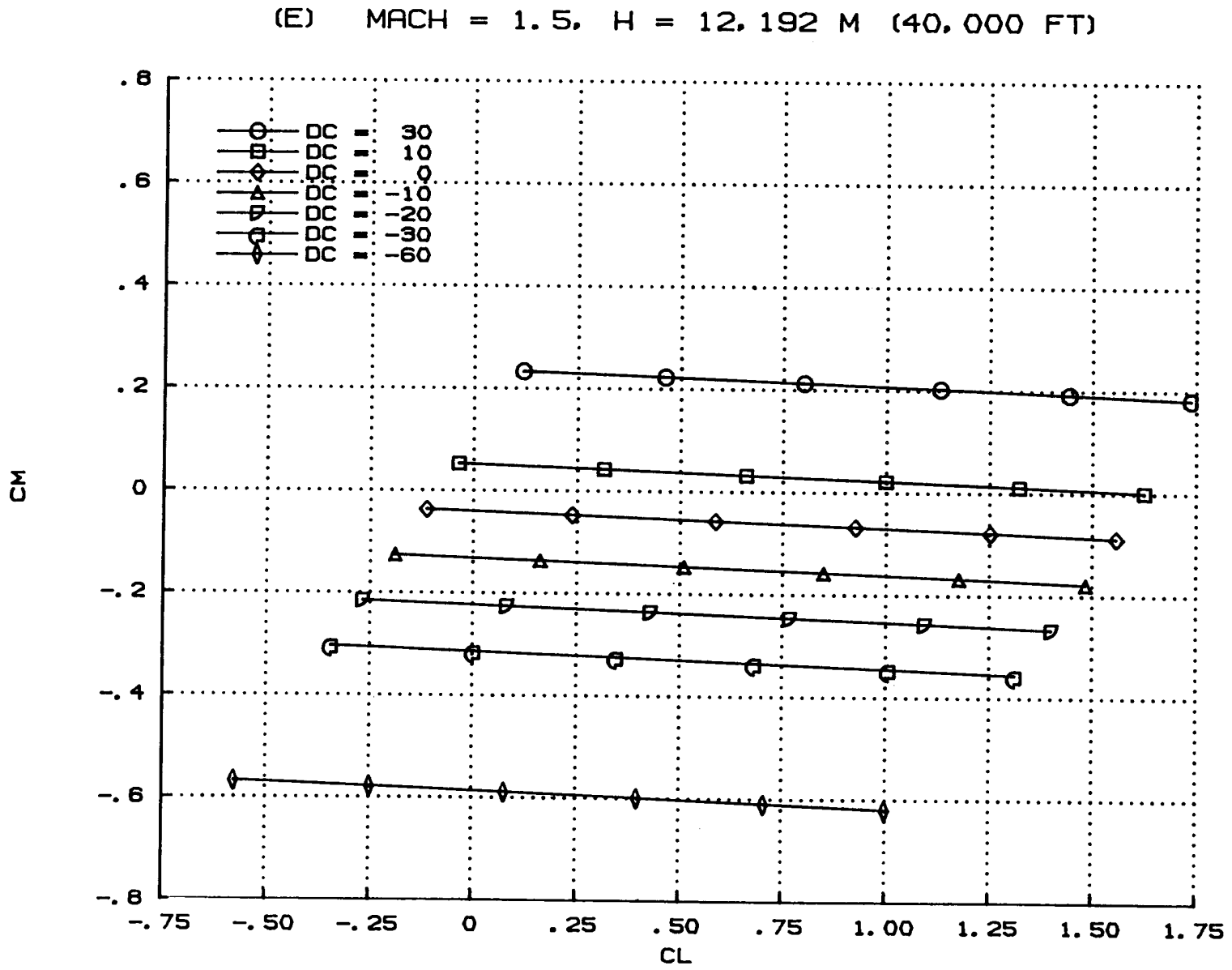

FIGURE 1. CM AS A FUNCTION OF CL. FLEXIBLE, VARYING DC.

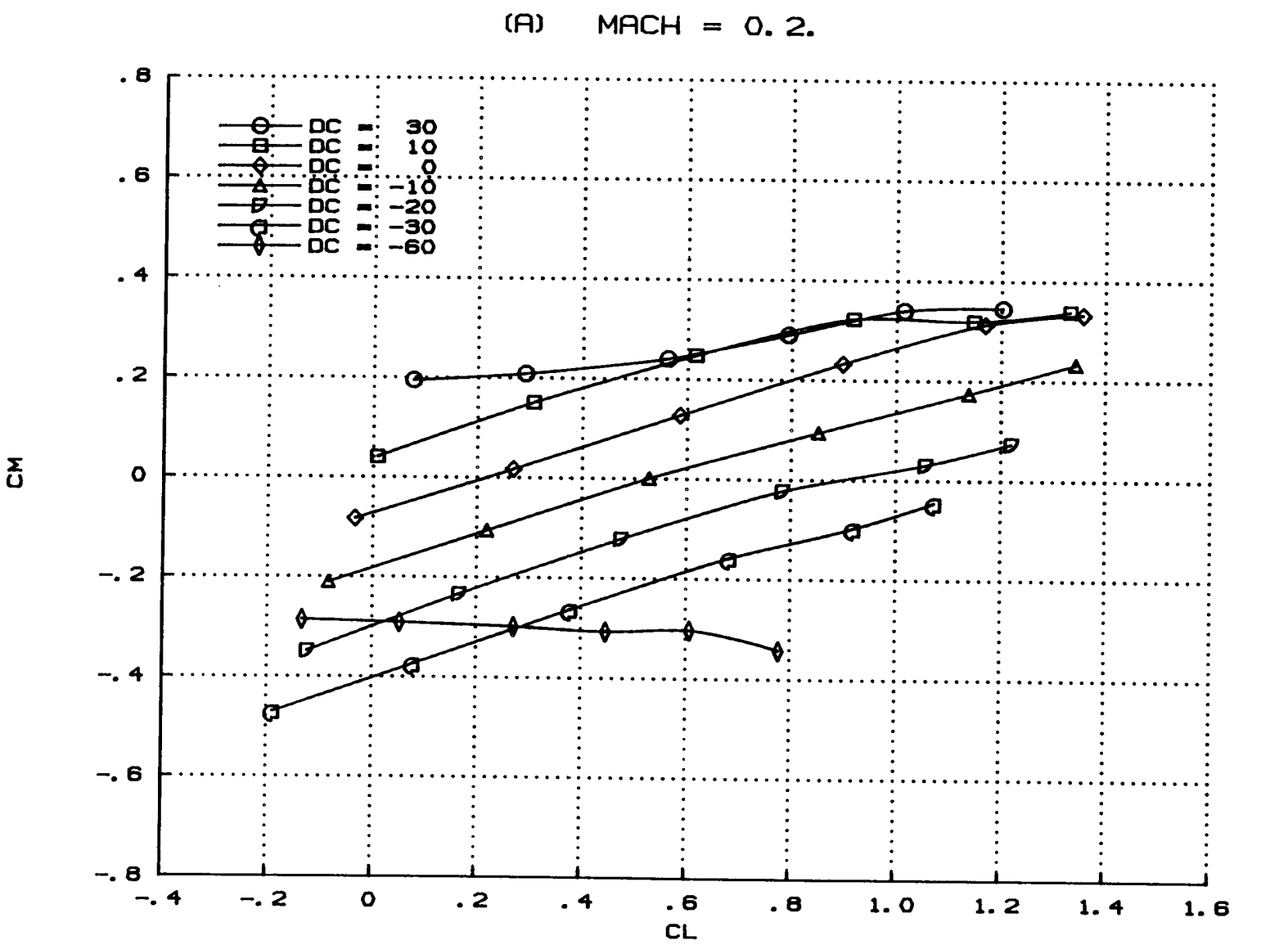

FIGURE 2. CM AS A FUNCTION OF CL. RIGID. VARYING DC.

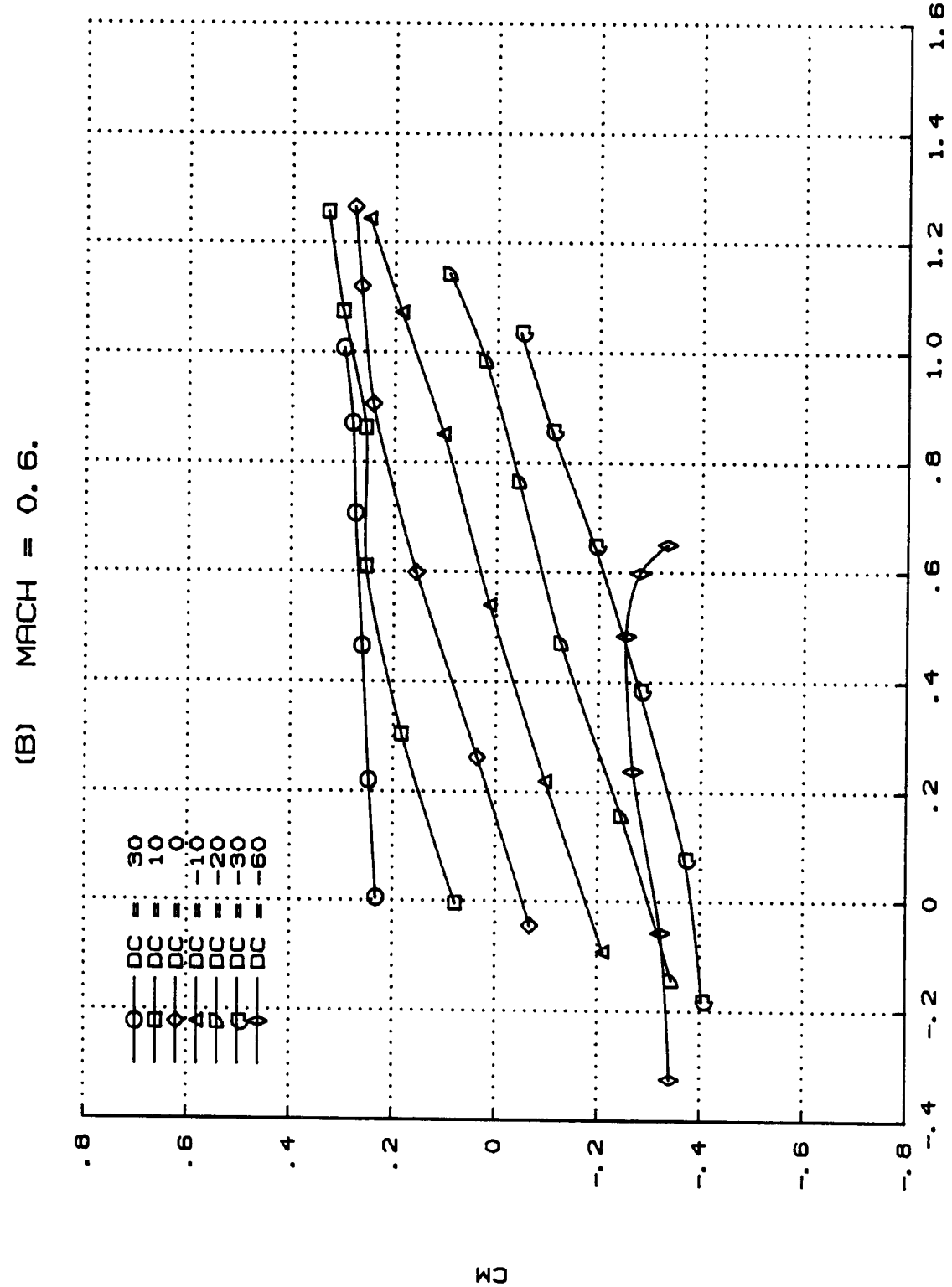

FIGURE 2. CM AS A FUNCTION OF CL. RIGID, VARYING DC.

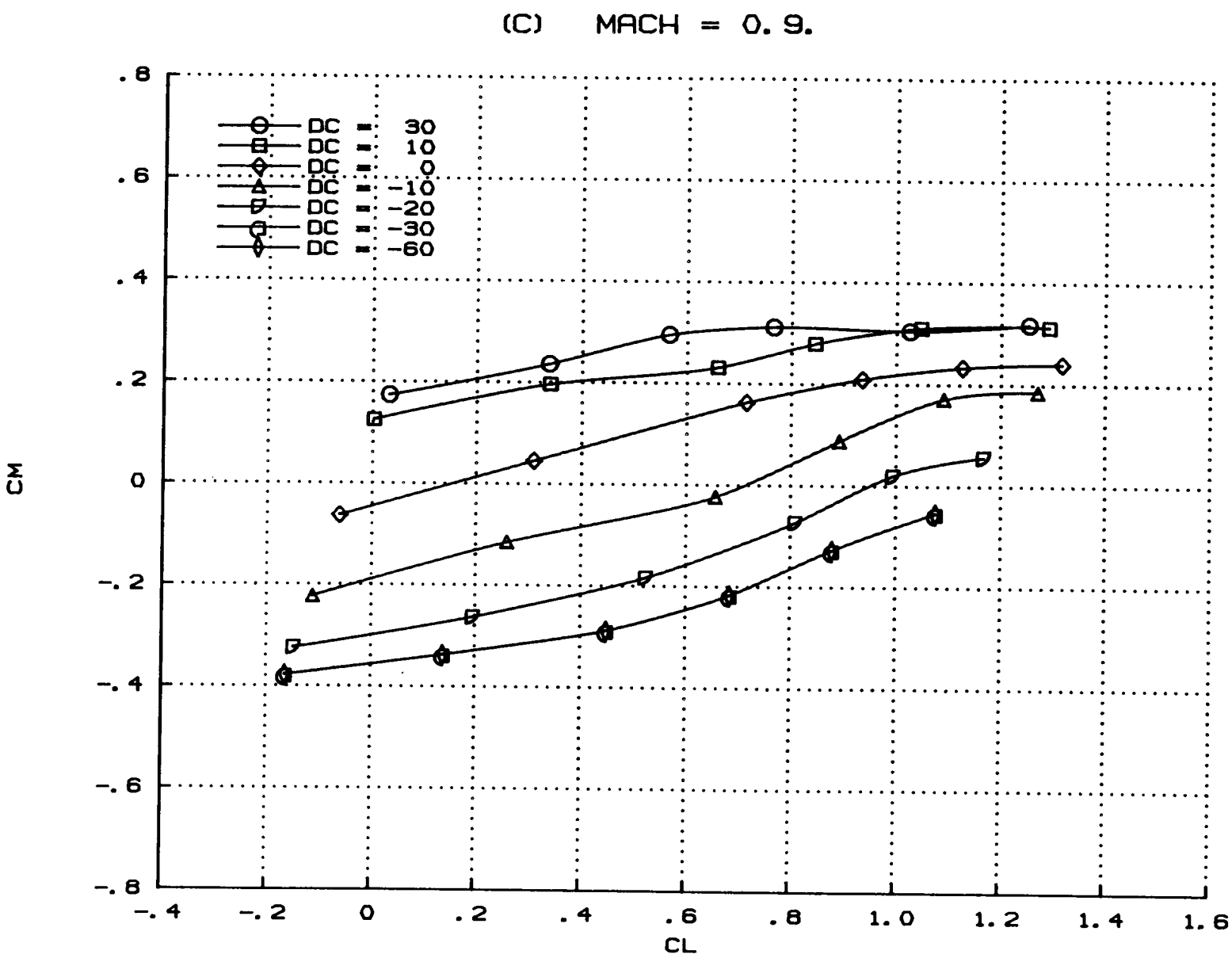

FIGURE 2. CM AS A FUNCTION OF CL. RIGID. VARYING DC.

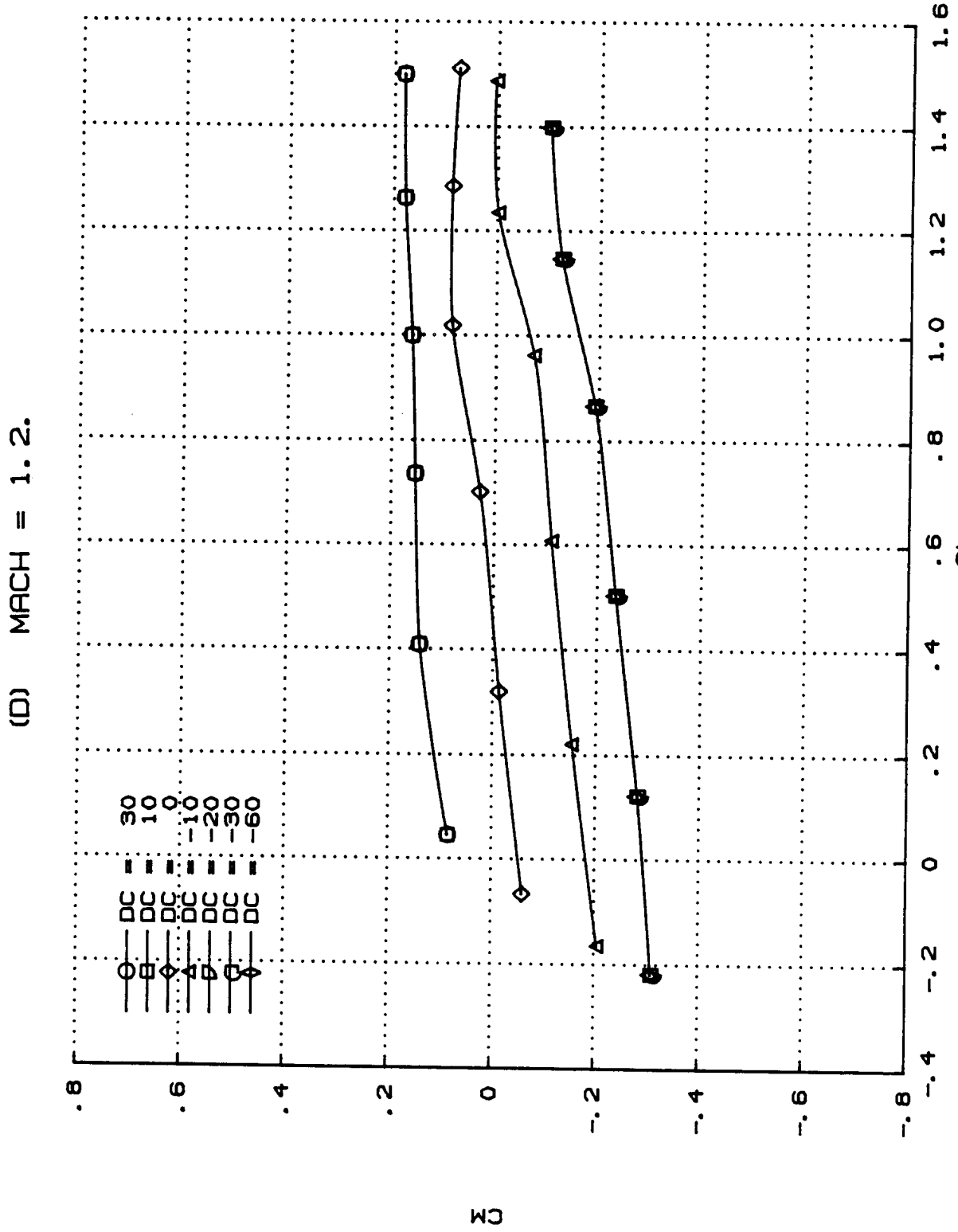

FIGURE 2. CM AS A FUNCTION OF CL. RIGID, VARYING DC.

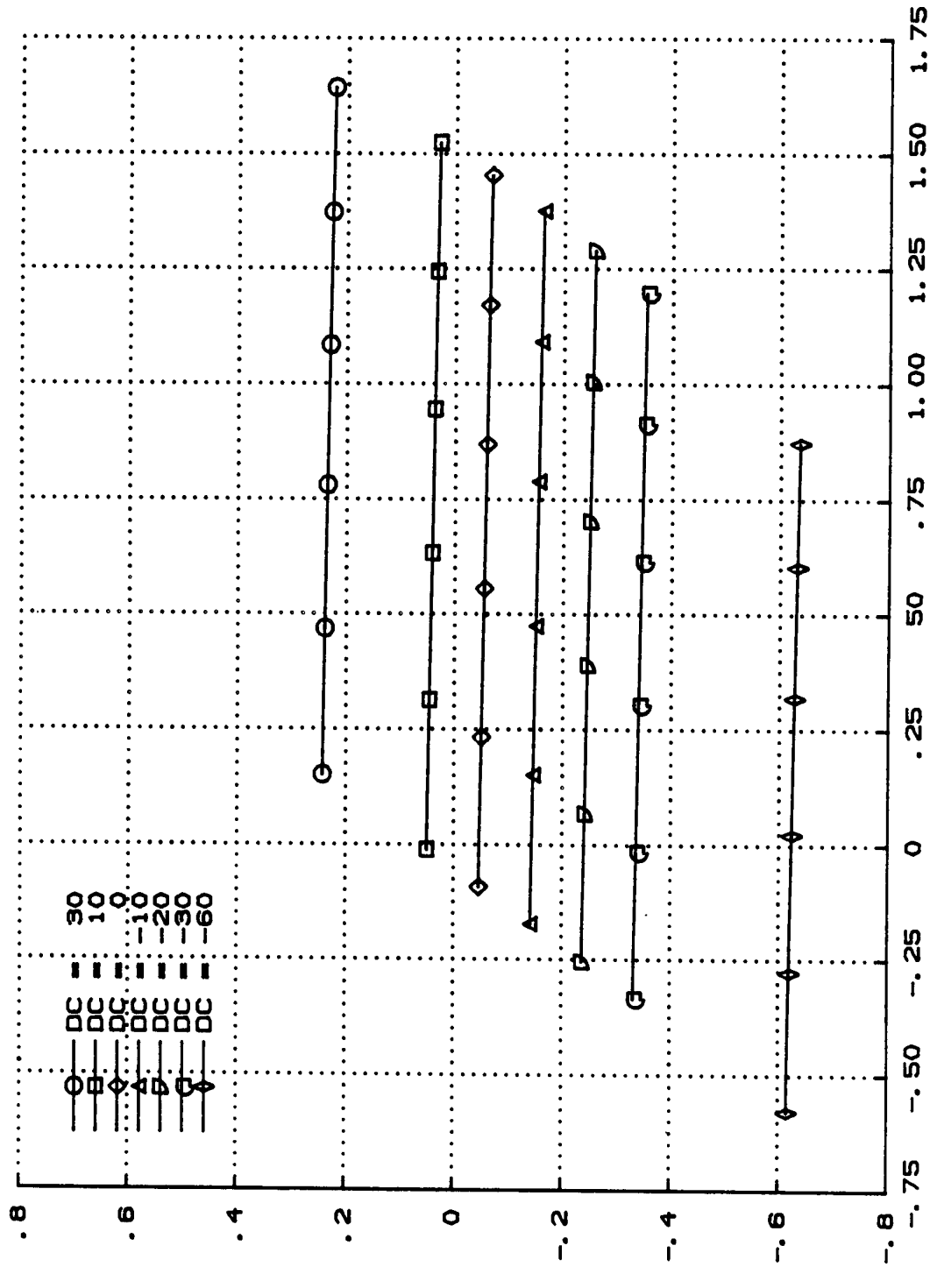

FIGURE 2. CM AS A FUNCTION OF CL. RIGID. VARYING DC.

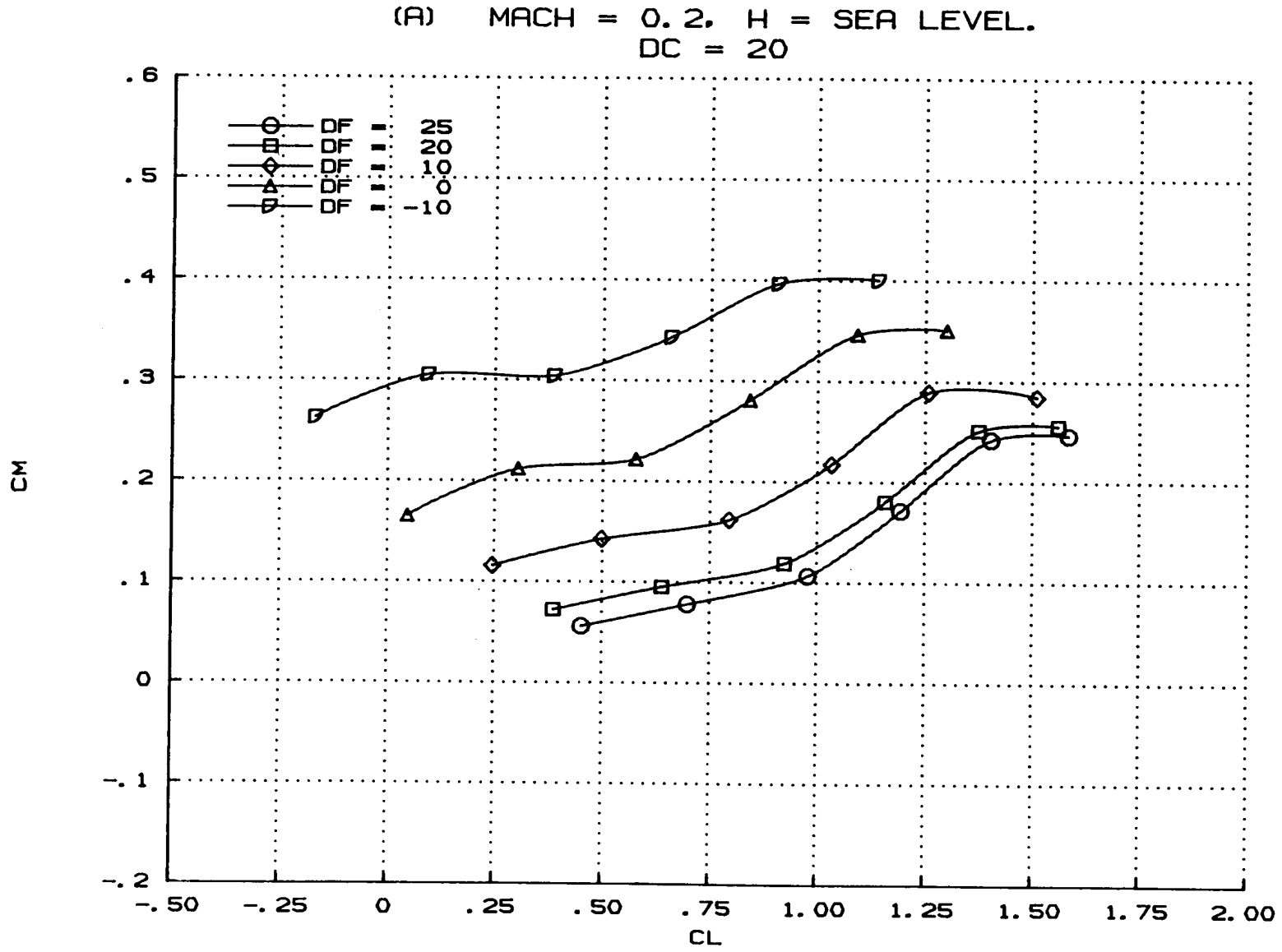

FIGURE 3. CM AS A FUNCTION OF CL. FLEXIBLE, VARYING DF.

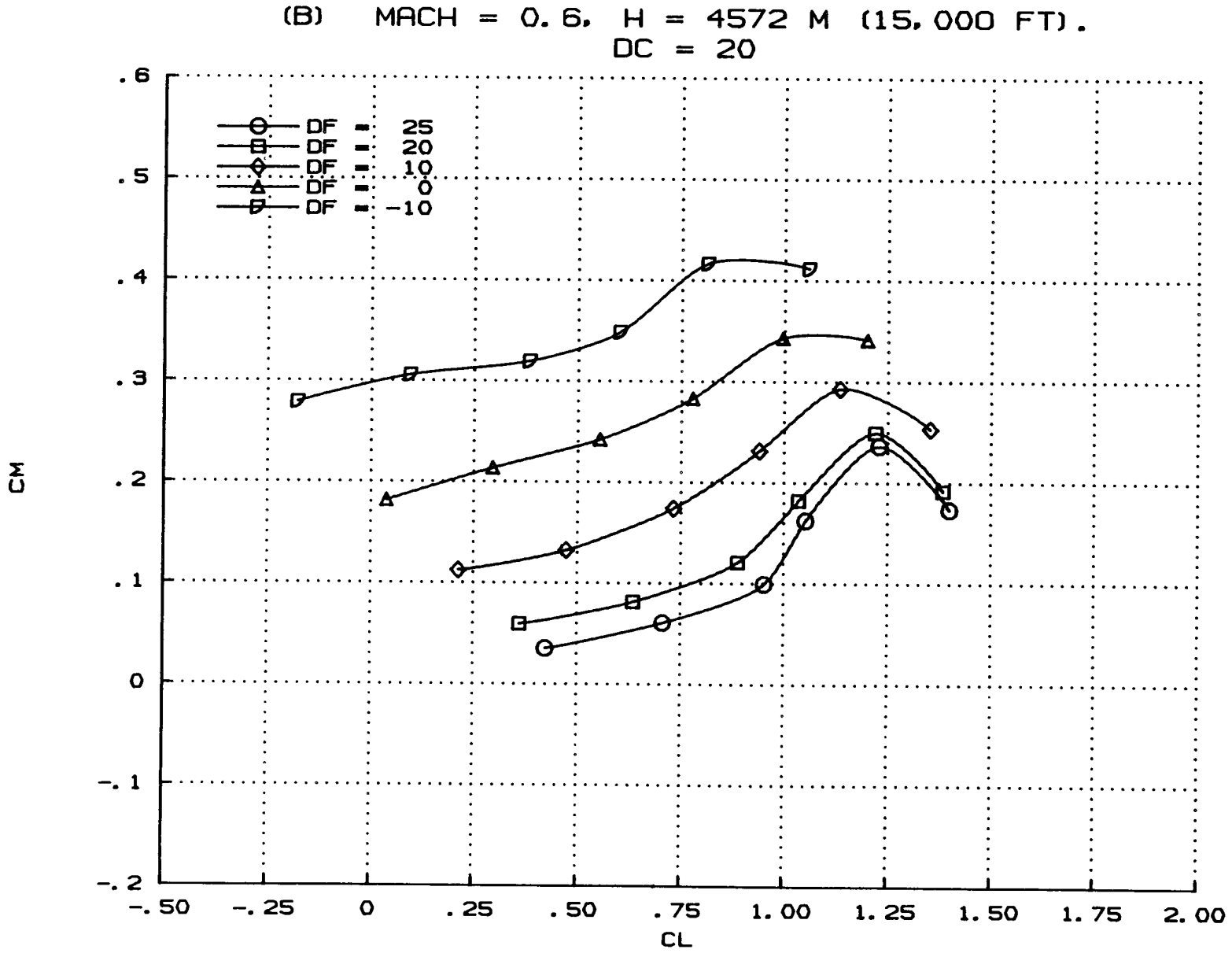

FIGURE 3. CM AS A FUNCTION OF CL. FLEXIBLE, VARYING DF.

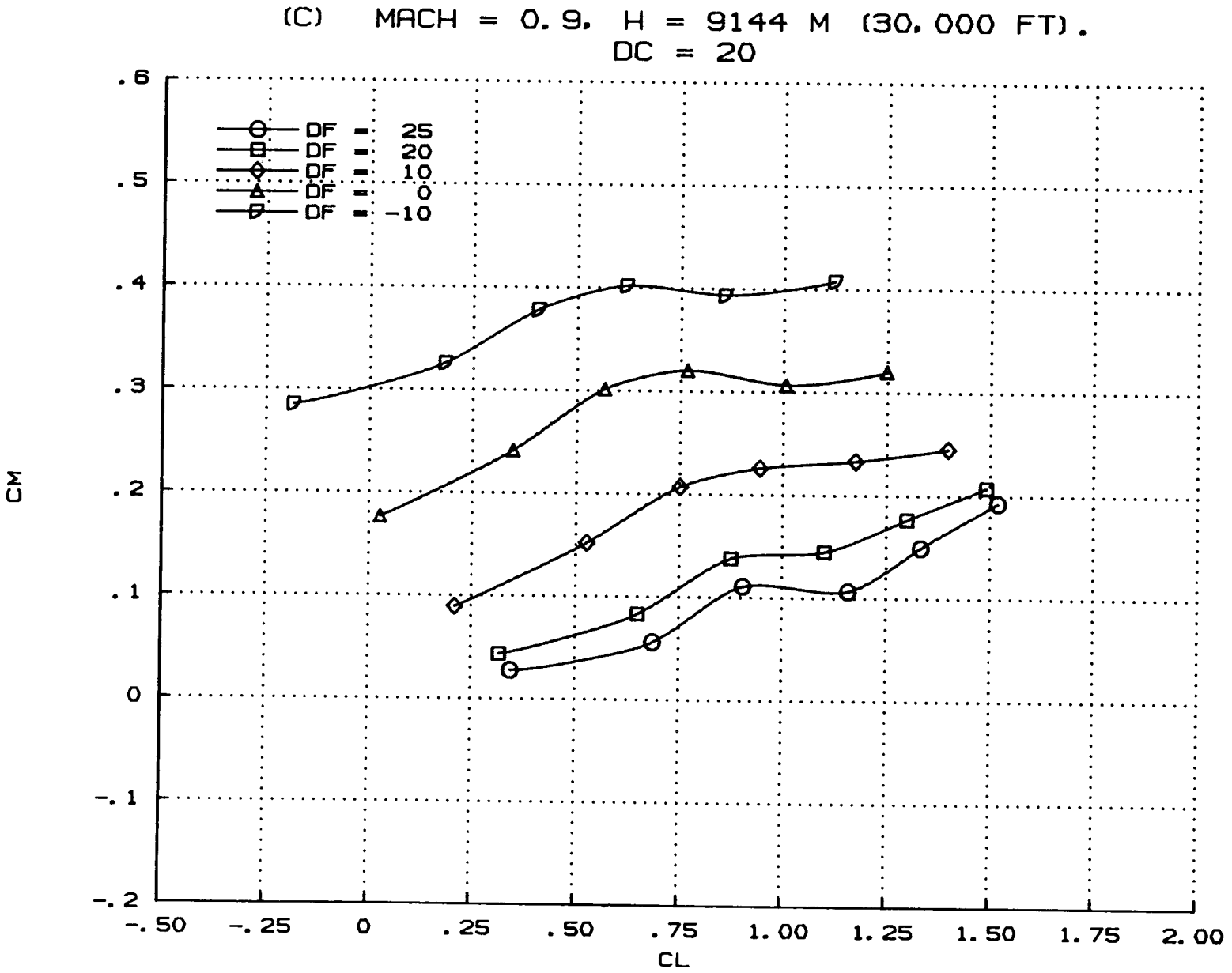

FIGURE 3. CM AS A FUNCTION OF CL. FLEXIBLE, VARYING DF.

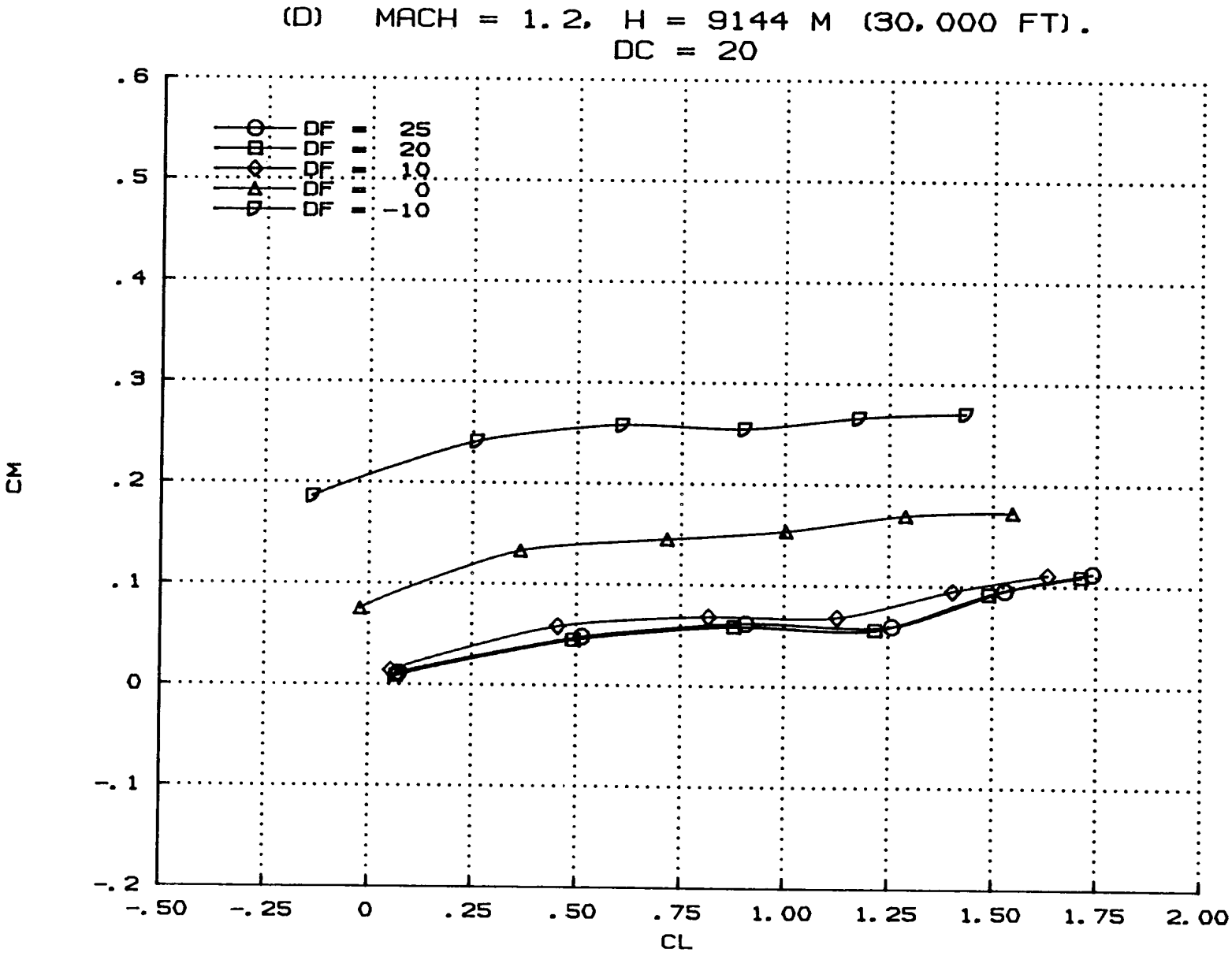

FIGURE 3. CM AS A FUNCTION OF CL. FLEXIBLE, VARYING DF.

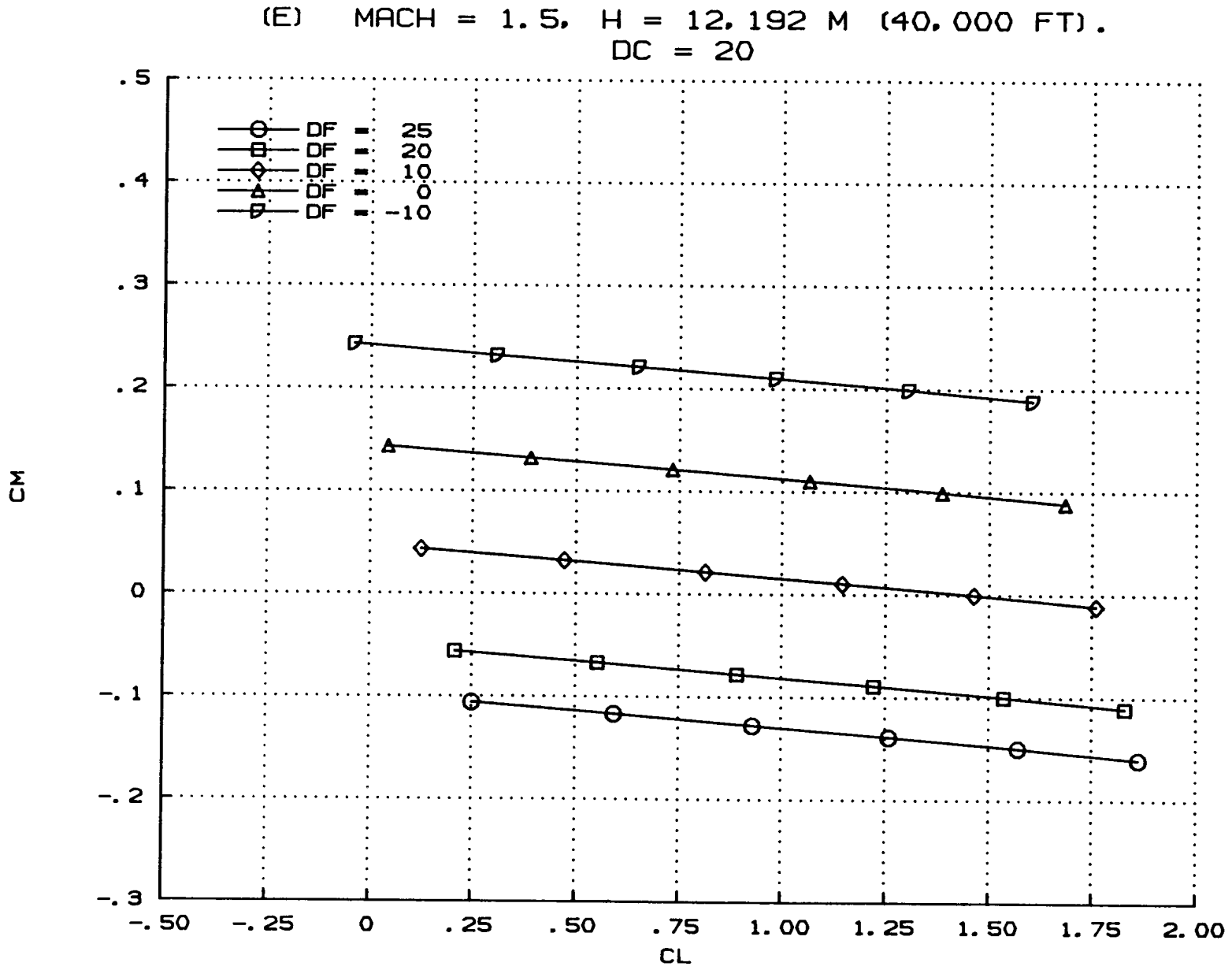

FIGURE 3. CM AS A FUNCTION OF CL. FLEXIBLE, VARYING DF.

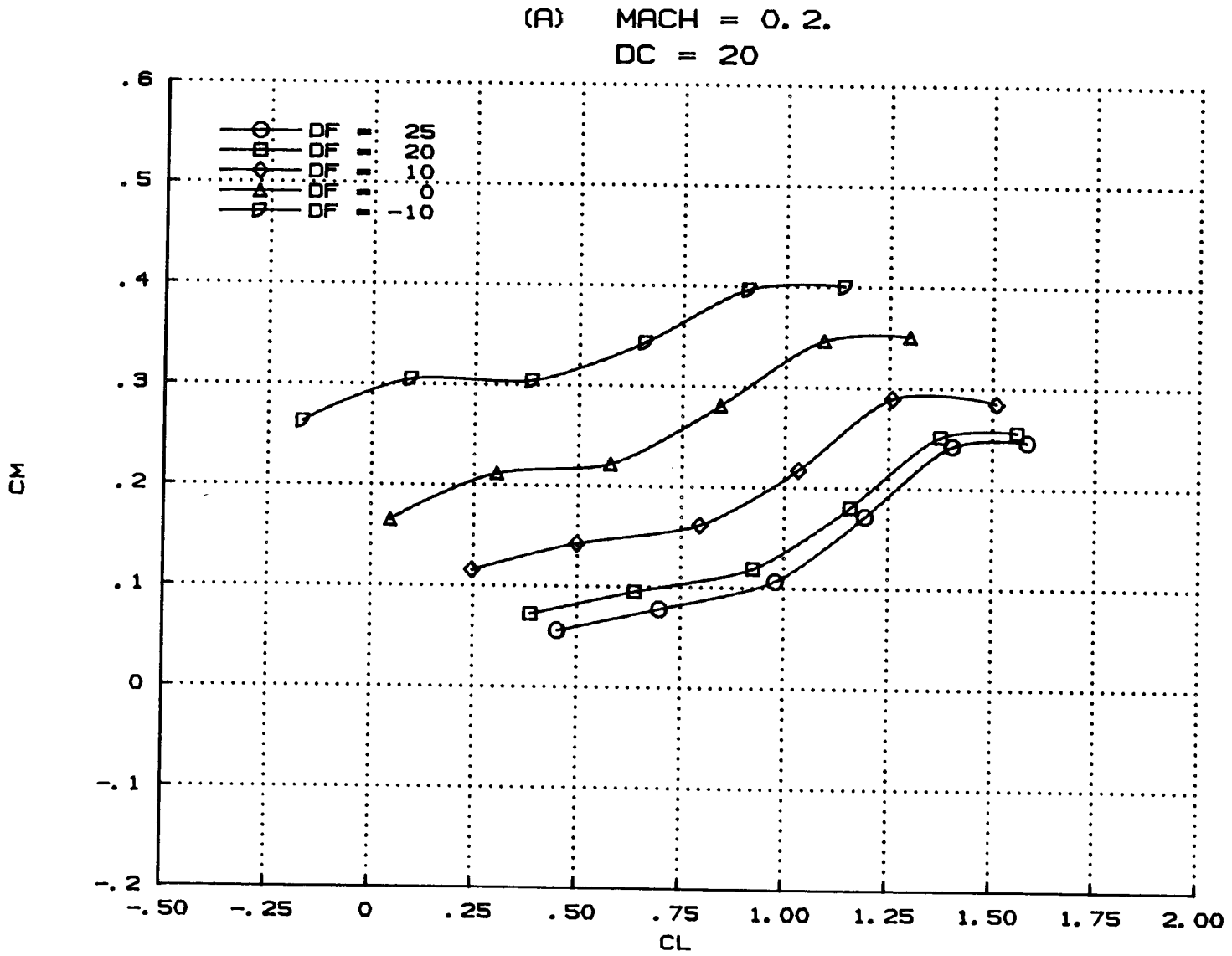

FIGURE 4. CM AS A FUNCTION OF CL. RIGID, VARYING DF.

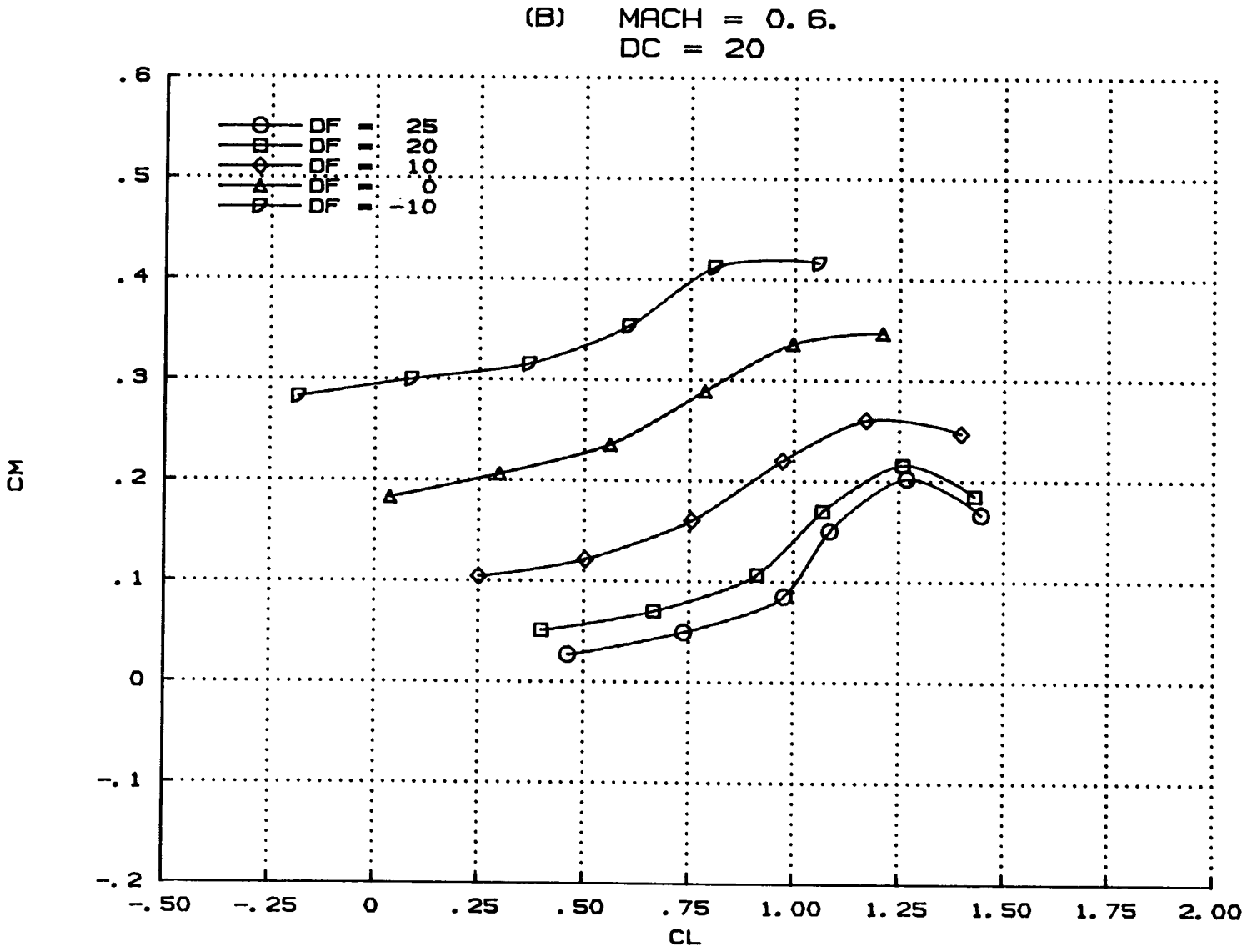

FIGURE 4. CM AS A FUNCTION OF CL. RIGID. VARYING DF.

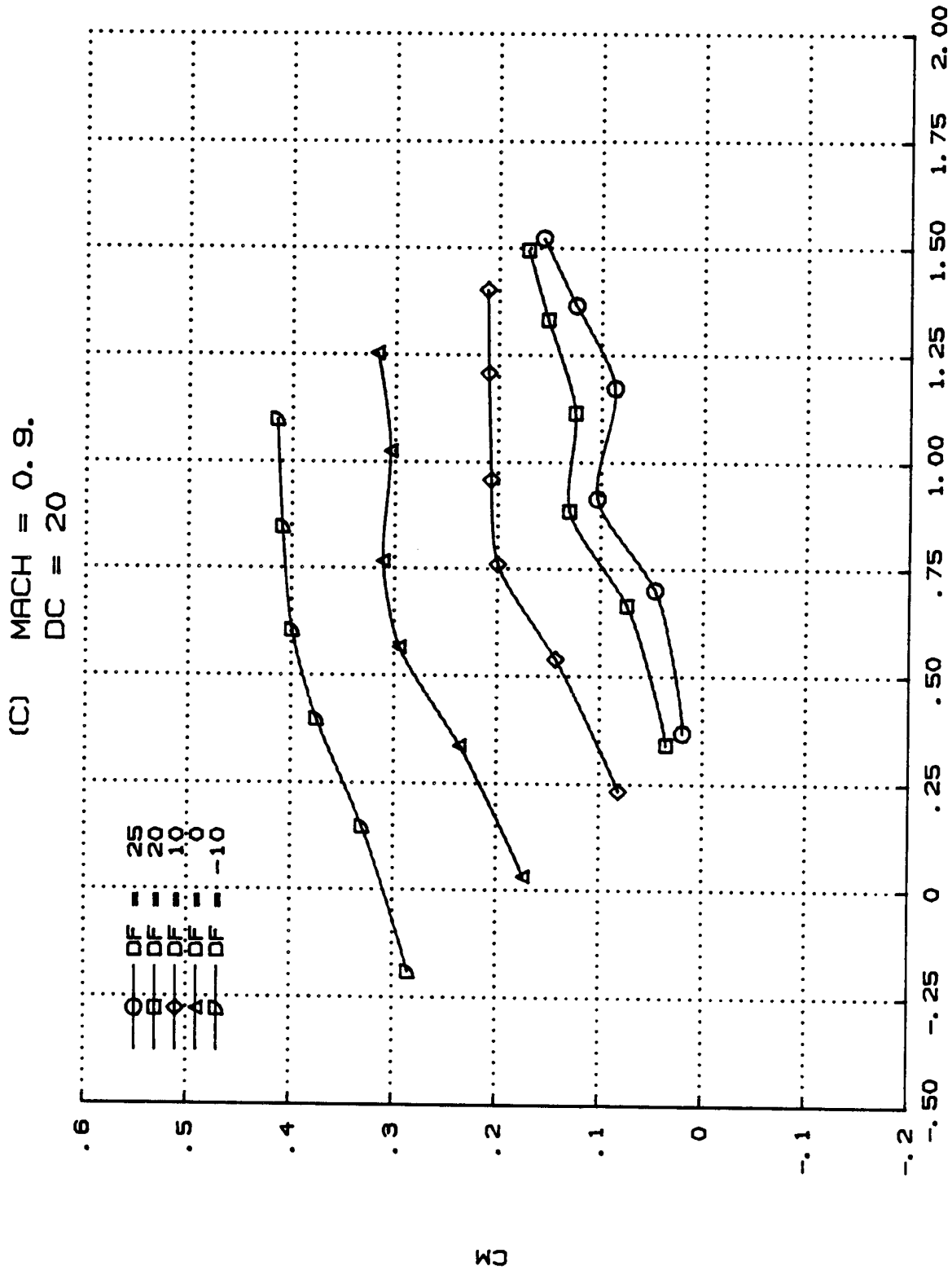

FIGURE 4. CM AS A FUNCTION OF CL. RIGID, VARYING DF.

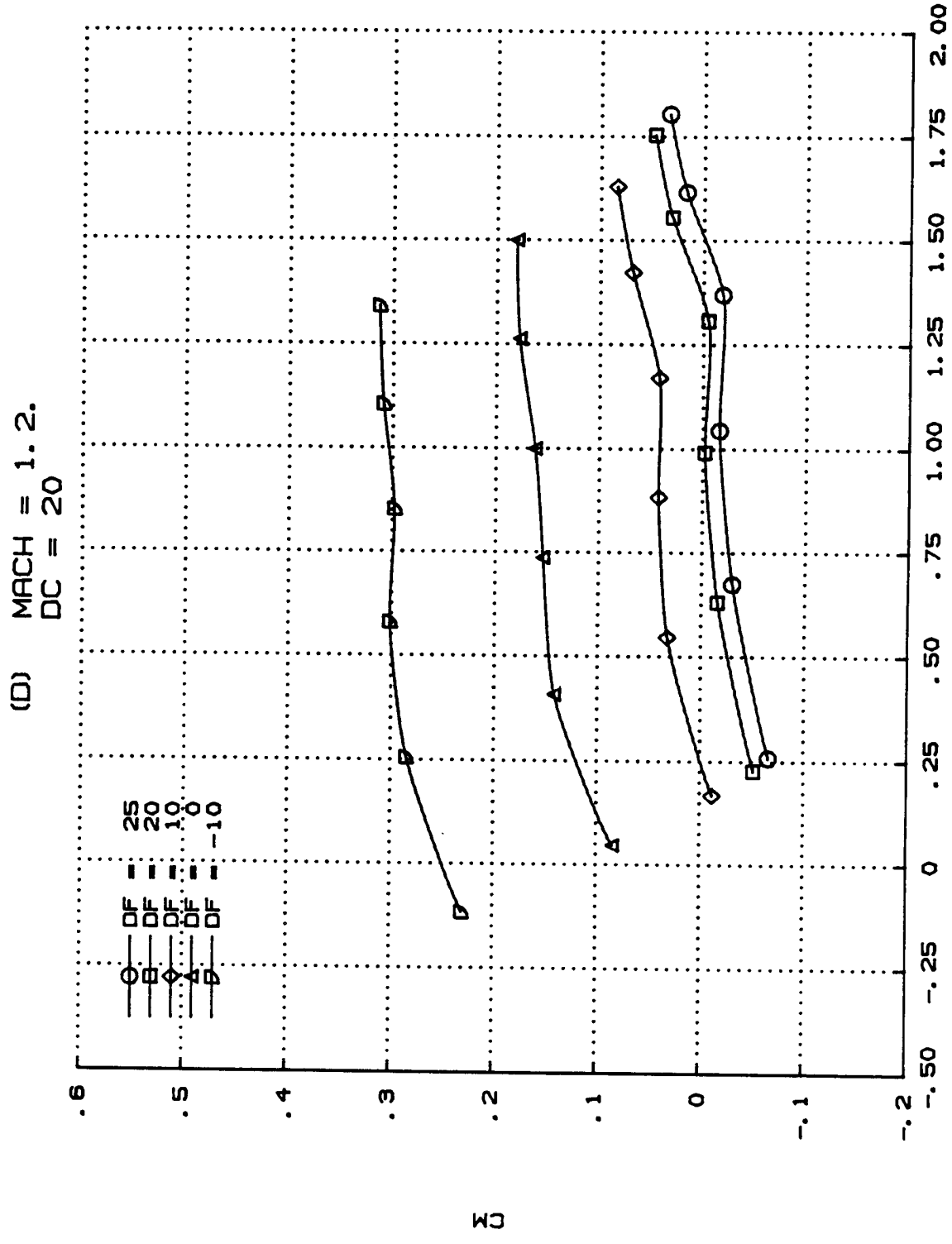

FIGURE 4. CM AS A FUNCTION OF CL. RIGID, VARYING DF.

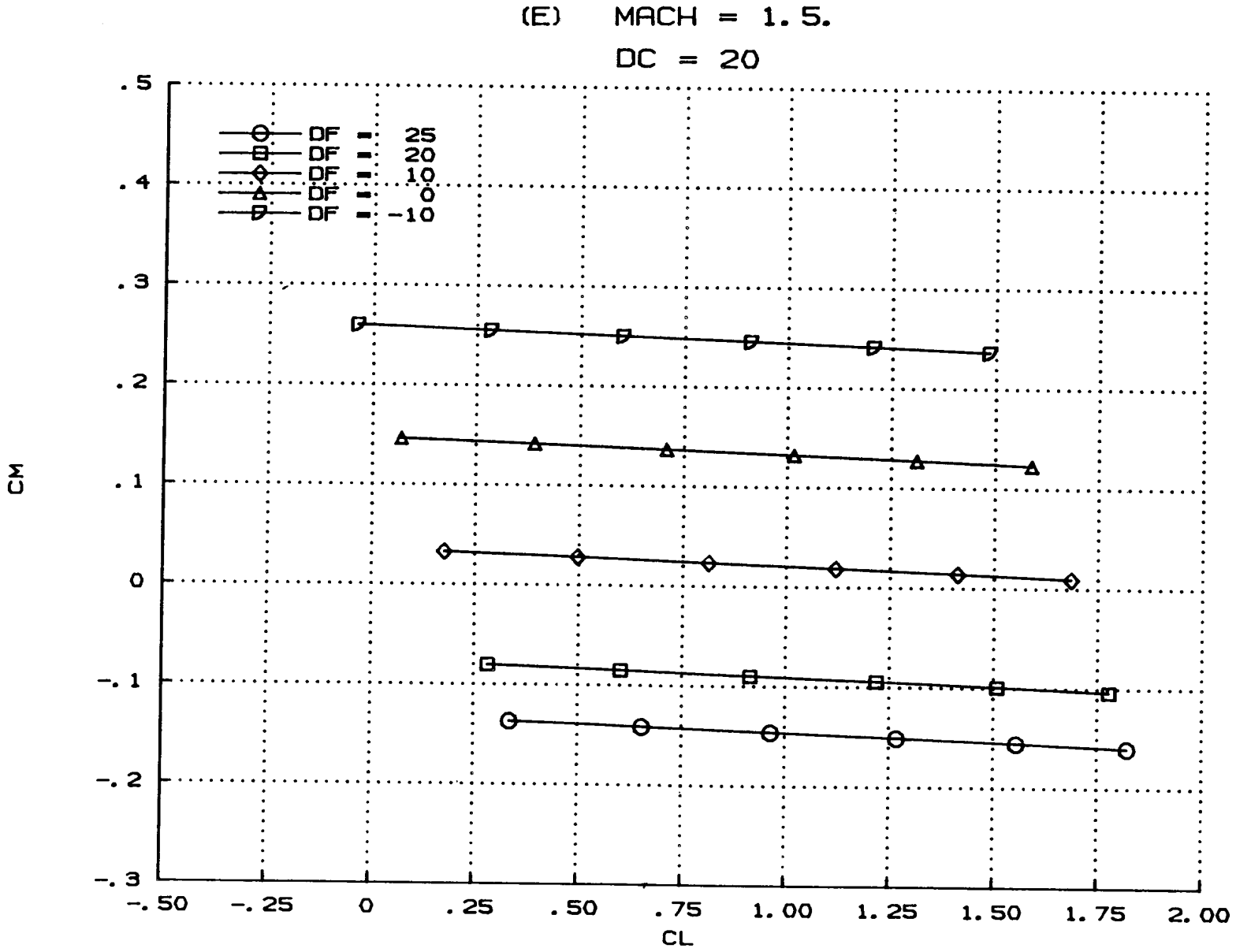

FIGURE 4. CM AS A FUNCTION OF CL. RIGID. VARYING DF.

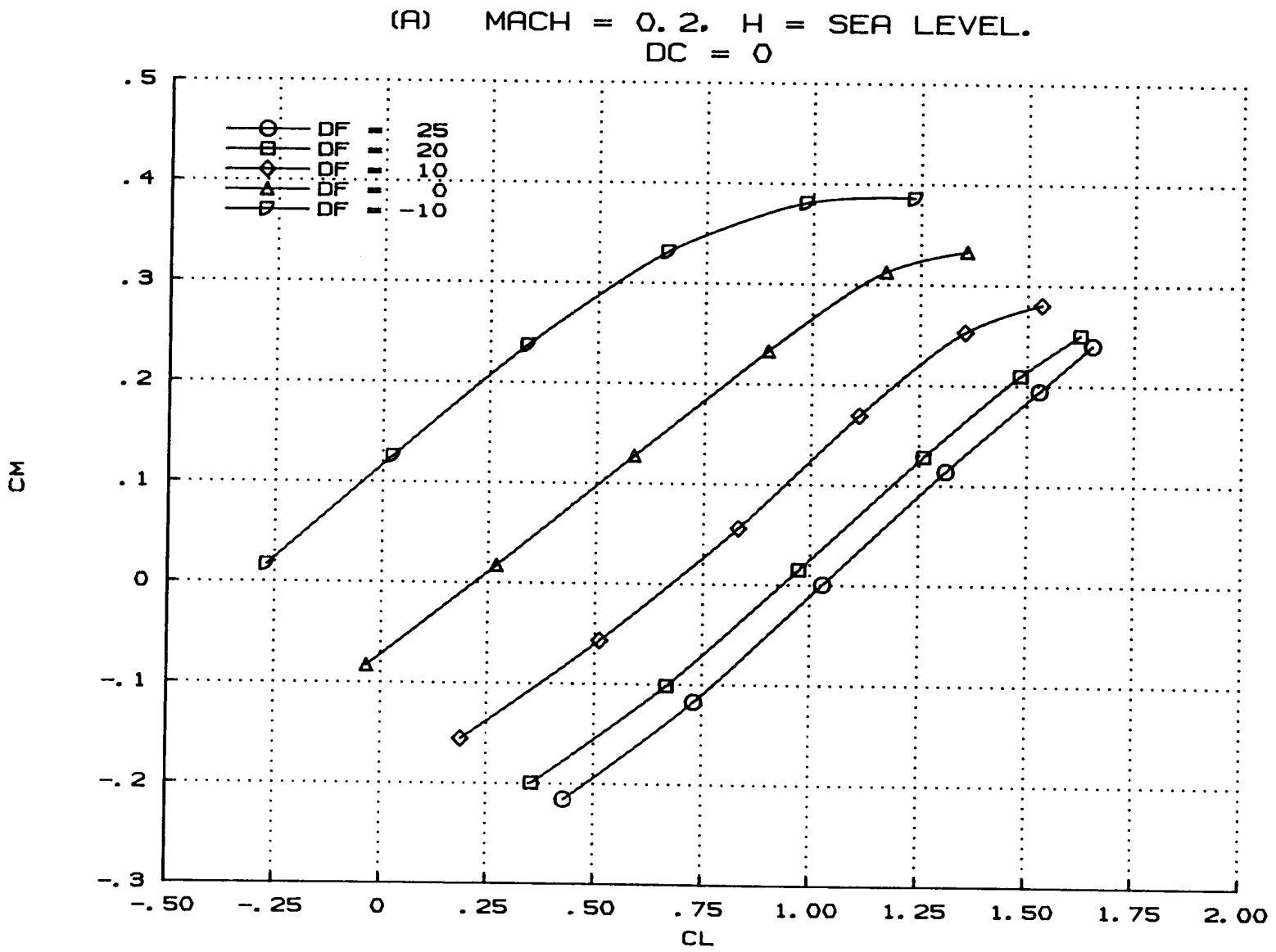

FIGURE 5. CM AS A FUNCTION OF CL. FLEXIBLE. VARYING DF.

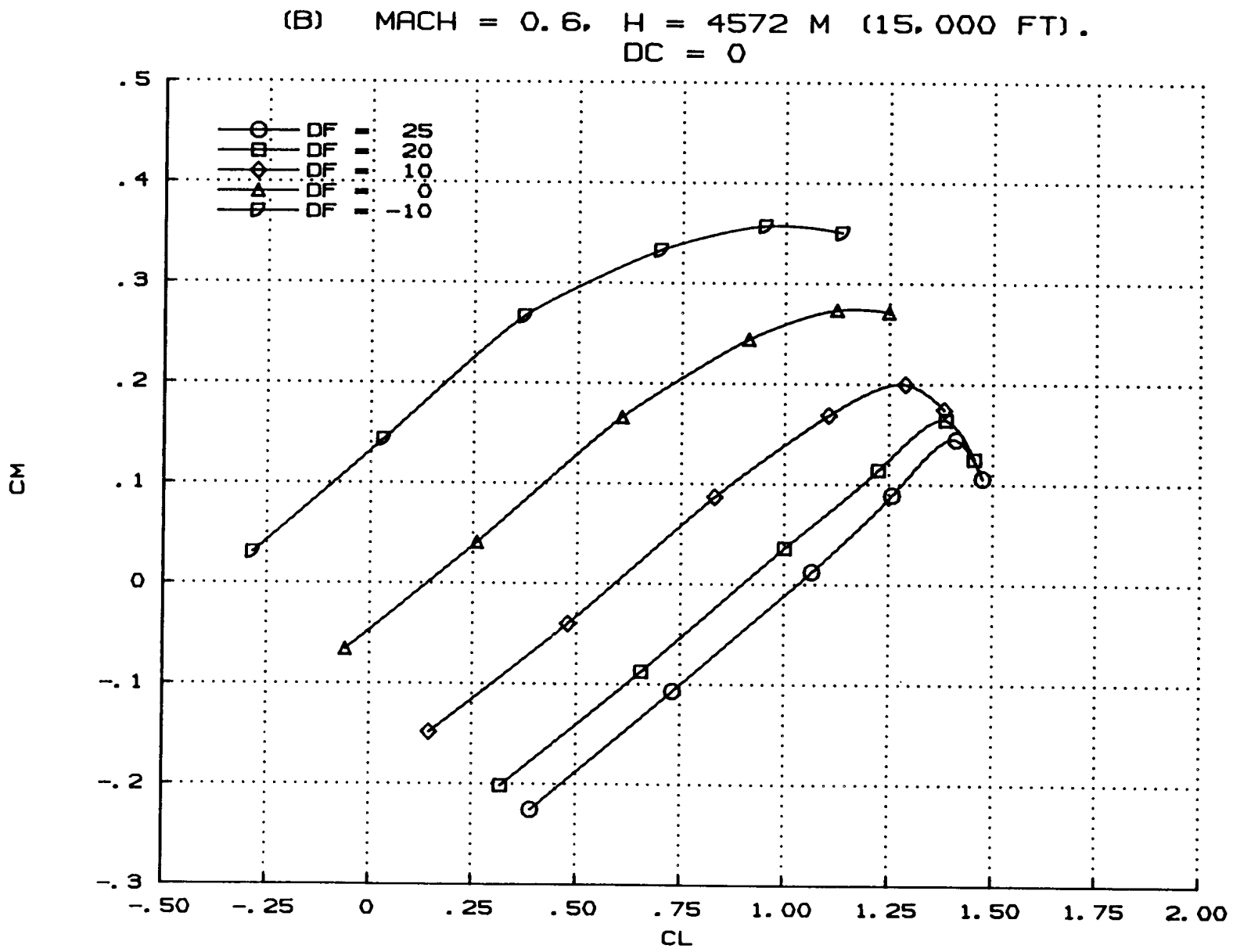

FIGURE 5. CM AS A FUNCTION OF CL. FLEXIBLE, VARYING DF.

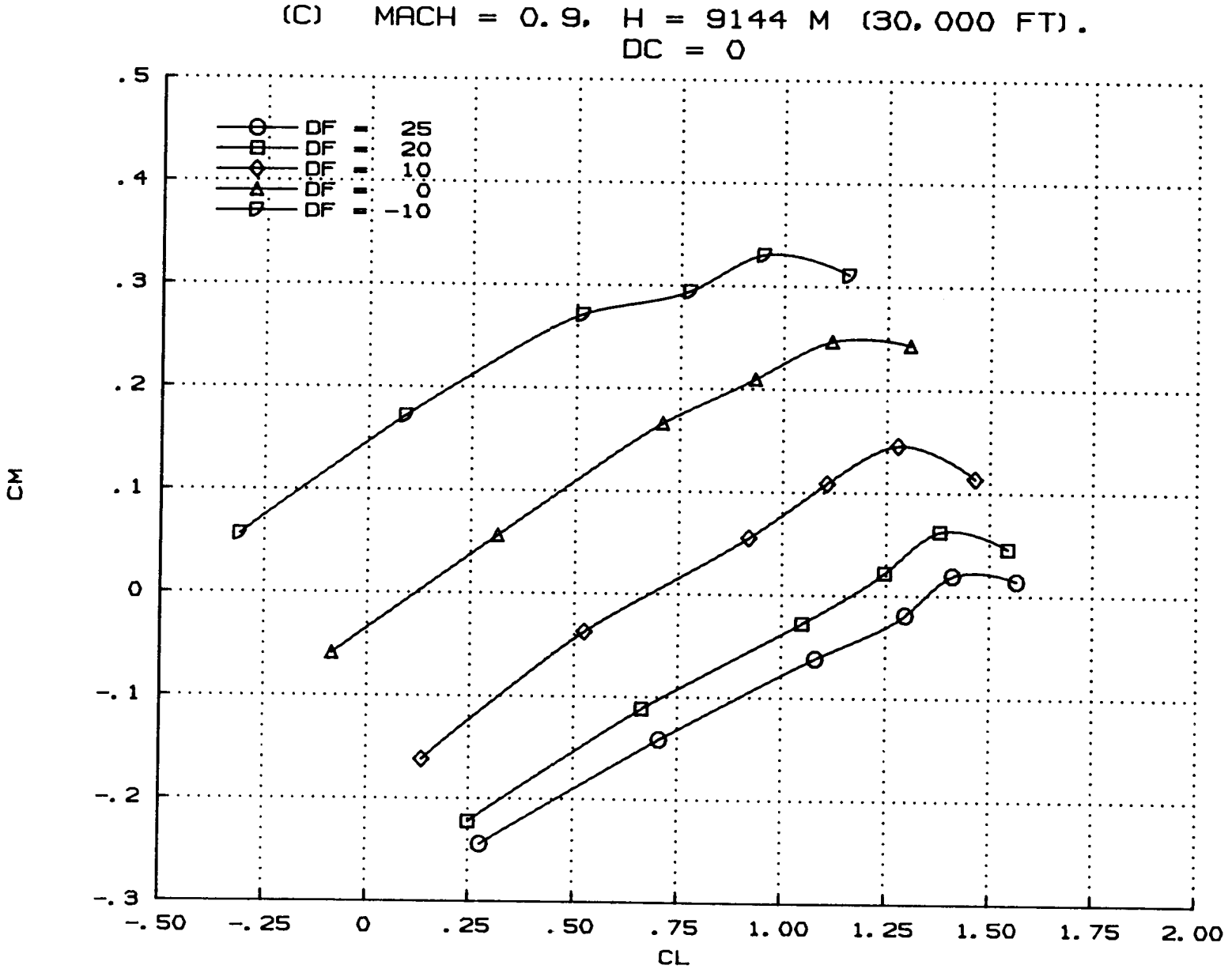

FIGURE 5. CM AS A FUNCTION OF CL. FLEXIBLE. VARYING DF.

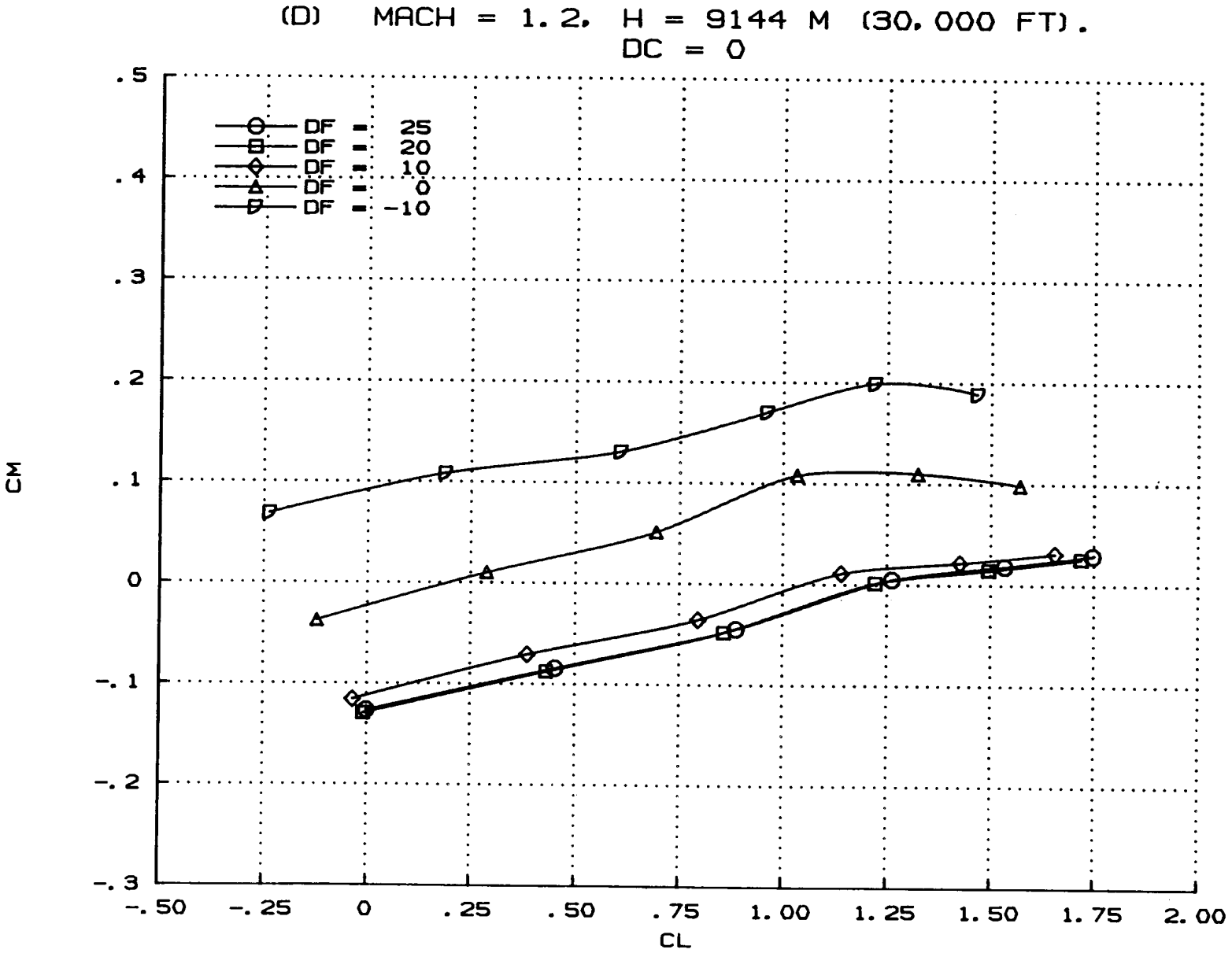

FIGURE 5. CM AS A FUNCTION OF CL. FLEXIBLE, VARYING DF.

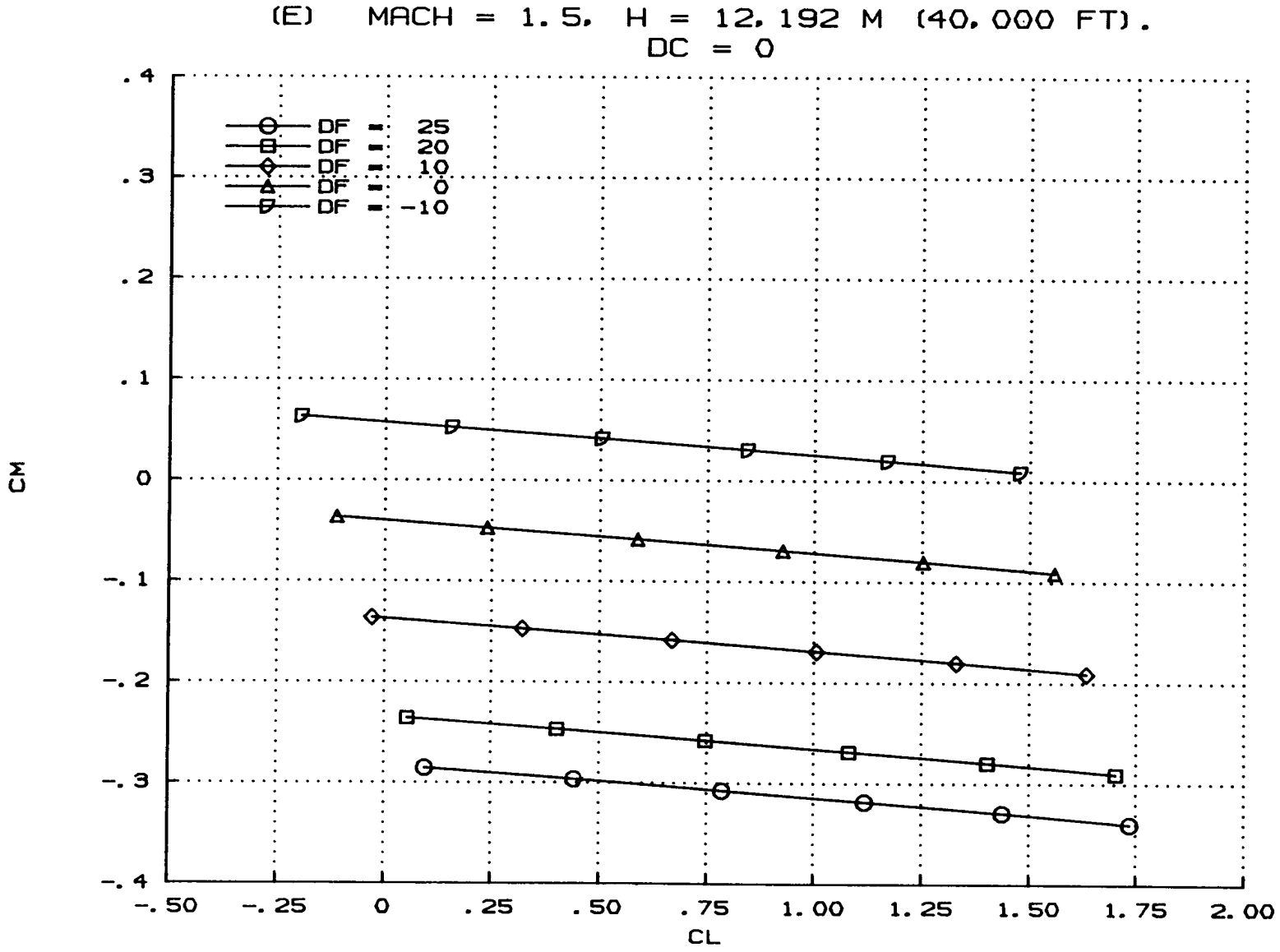

FIGURE 5. CM AS A FUNCTION OF CL. FLEXIBLE, VARYING DF.

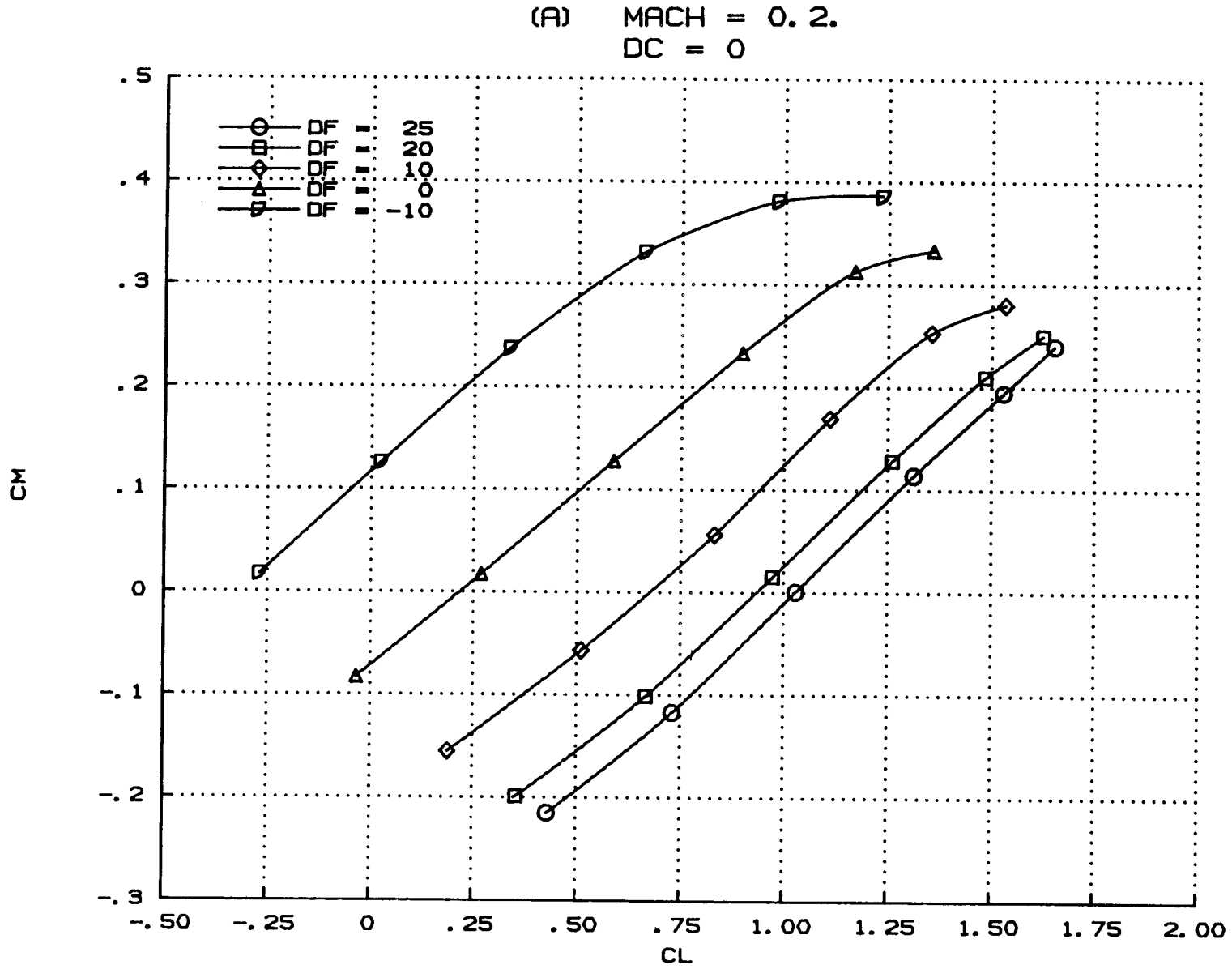

FIGURE 6. CM AS A FUNCTION OF CL. RIGID. VARYING DF.

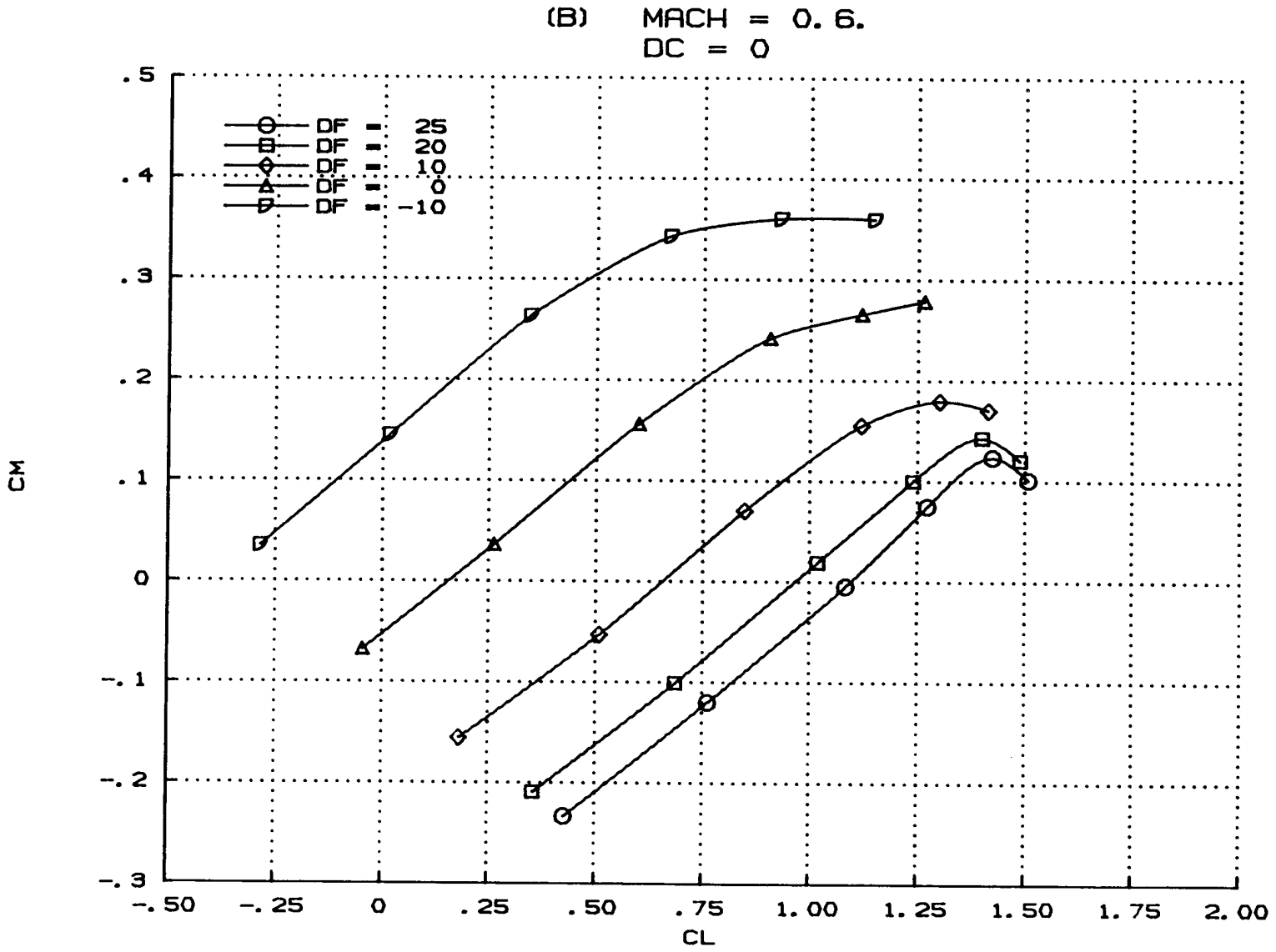

FIGURE 6. CM AS A FUNCTION OF CL. RIGID. VARYING DF.

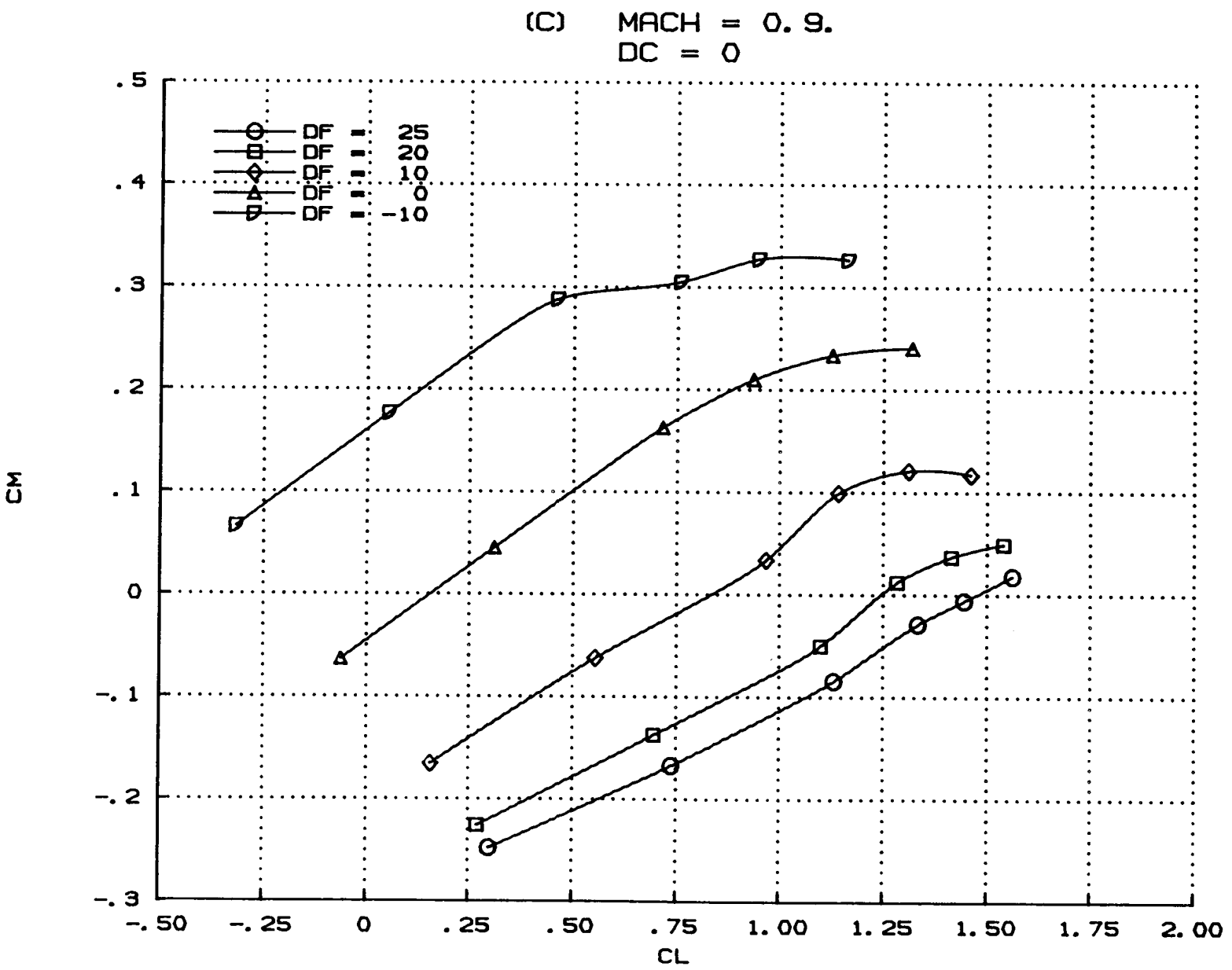

FIGURE 6. CM AS A FUNCTION OF CL. RIGID. VARYING DF.

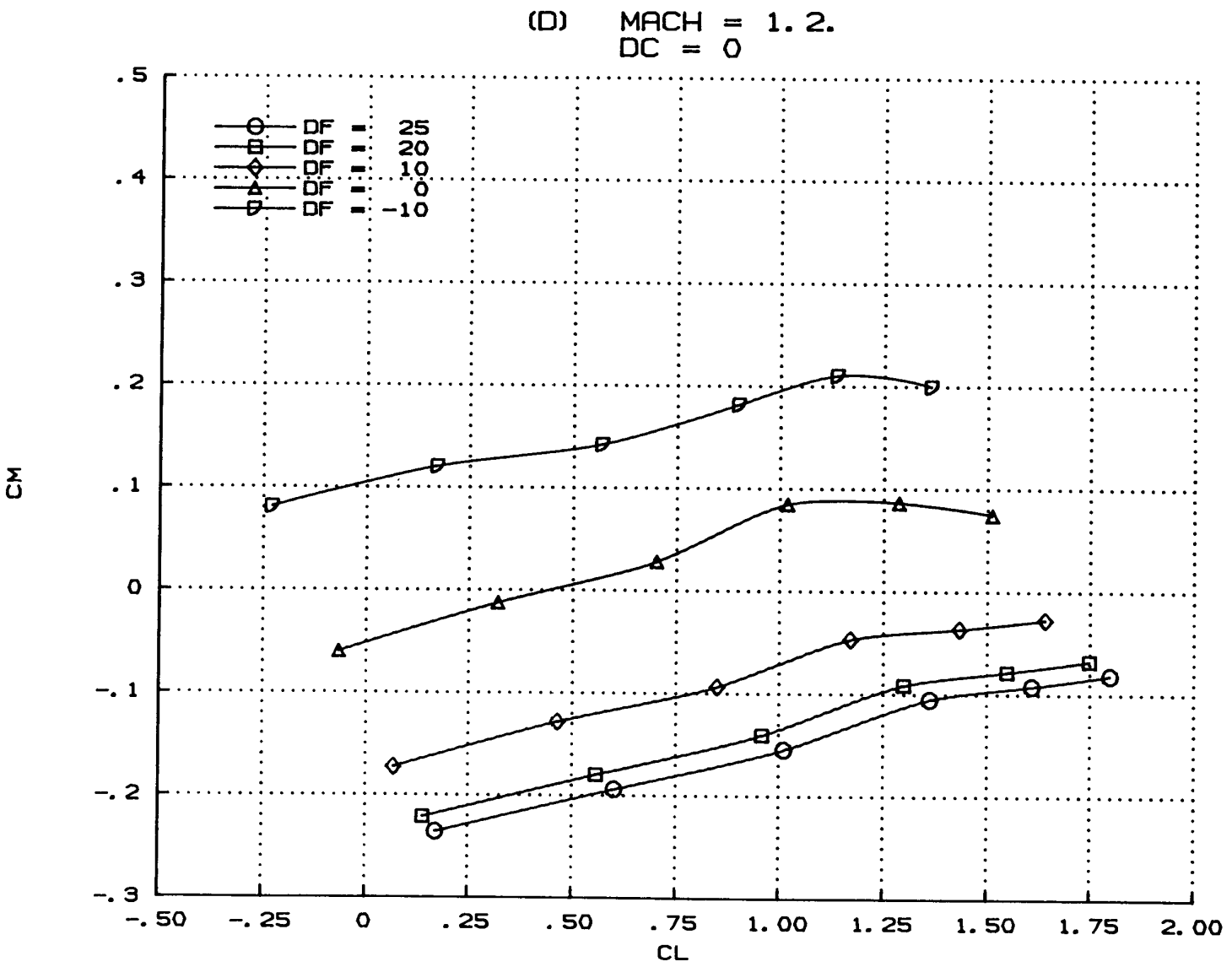

FIGURE 6. CM AS A FUNCTION OF CL. RIGID, VARYING DF.

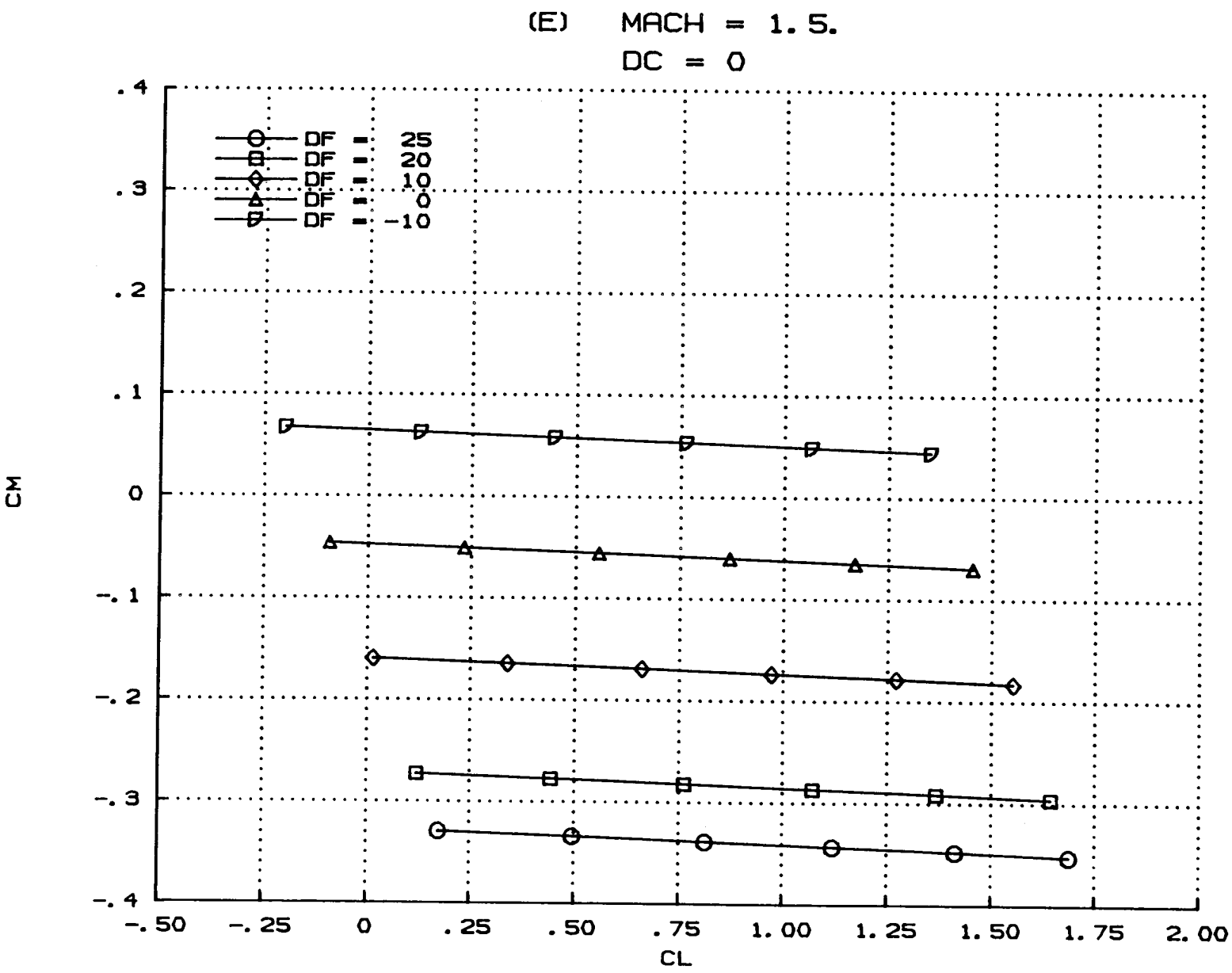

FIGURE 6. CM AS A FUNCTION OF CL. RIGID. VARYING DF.

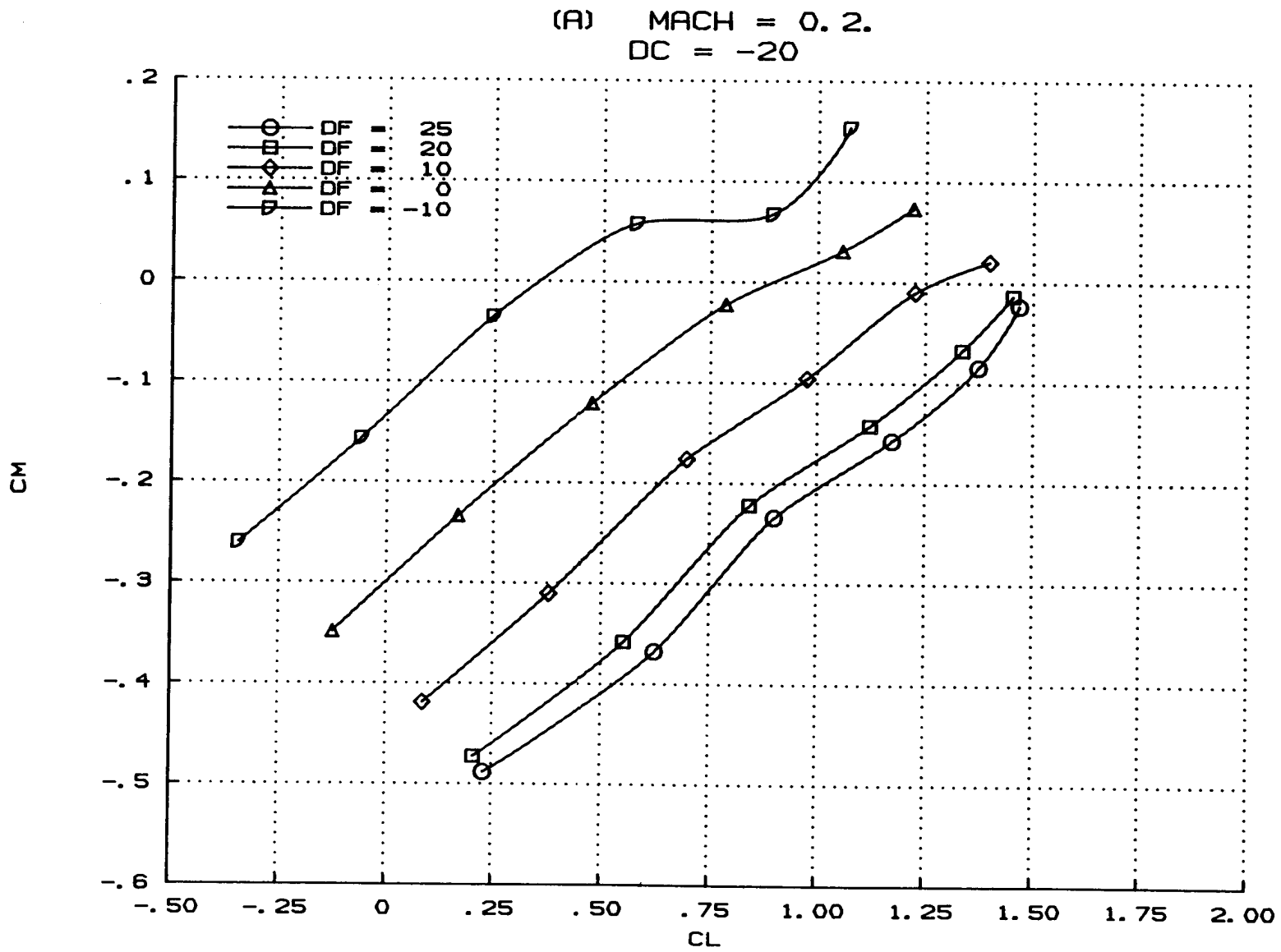

FIGURE 7. CM AS A FUNCTION OF CL. FLEXIBLE. VARYING DF.

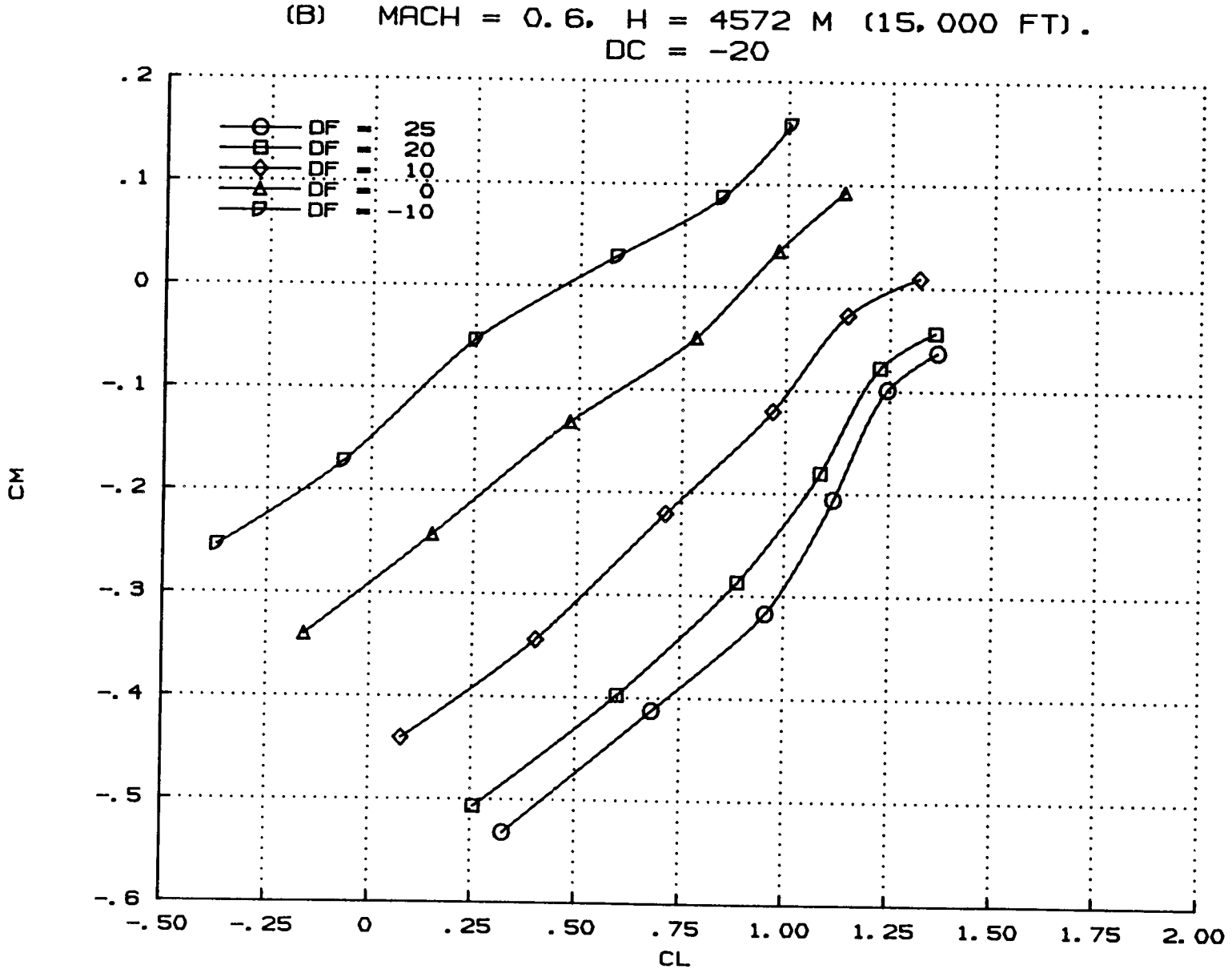

FIGURE 7. CM AS A FUNCTION OF CL. FLEXIBLE, VARYING DF.

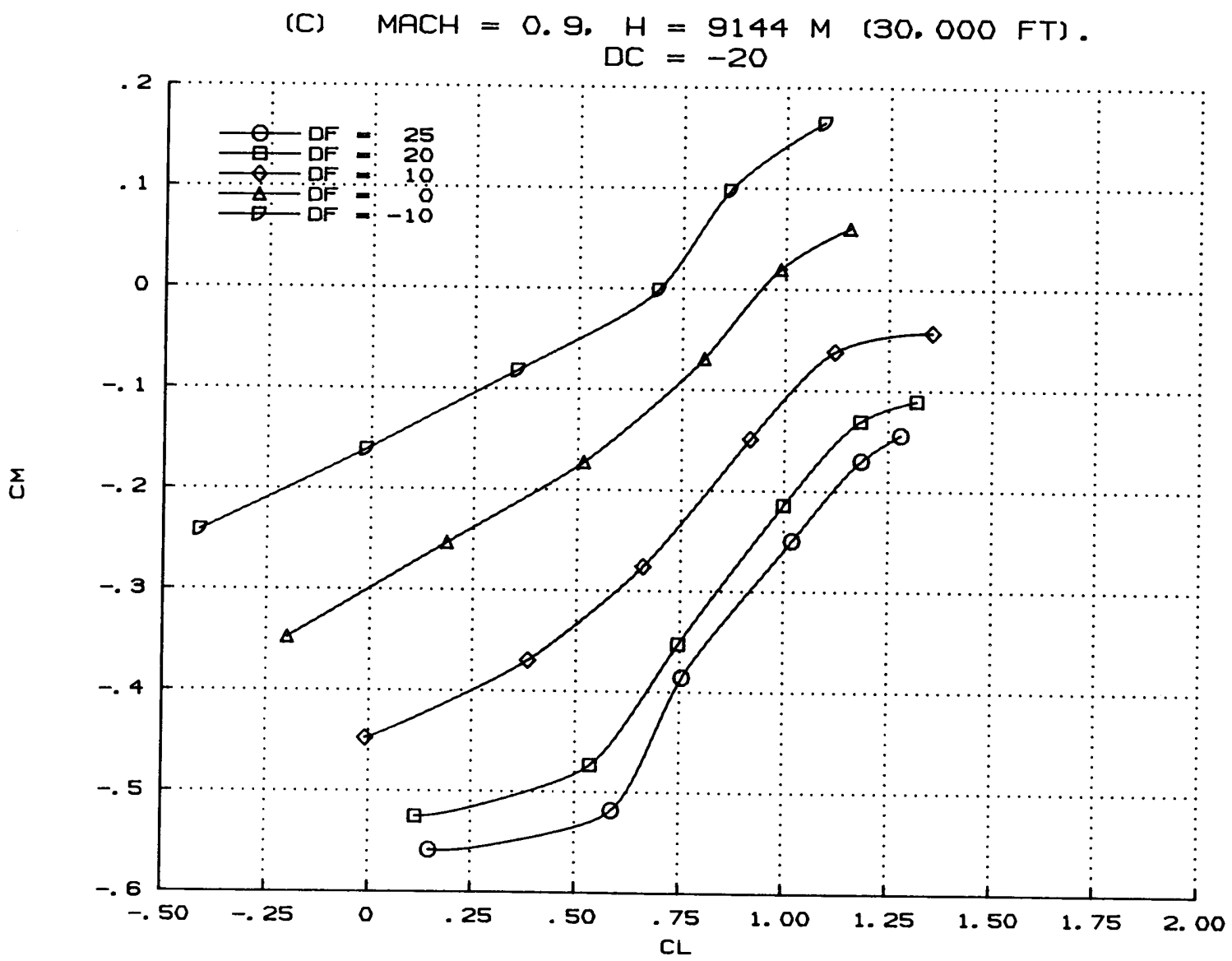

FIGURE 7. CM AS A FUNCTION OF CL. FLEXIBLE. VARYING DF.

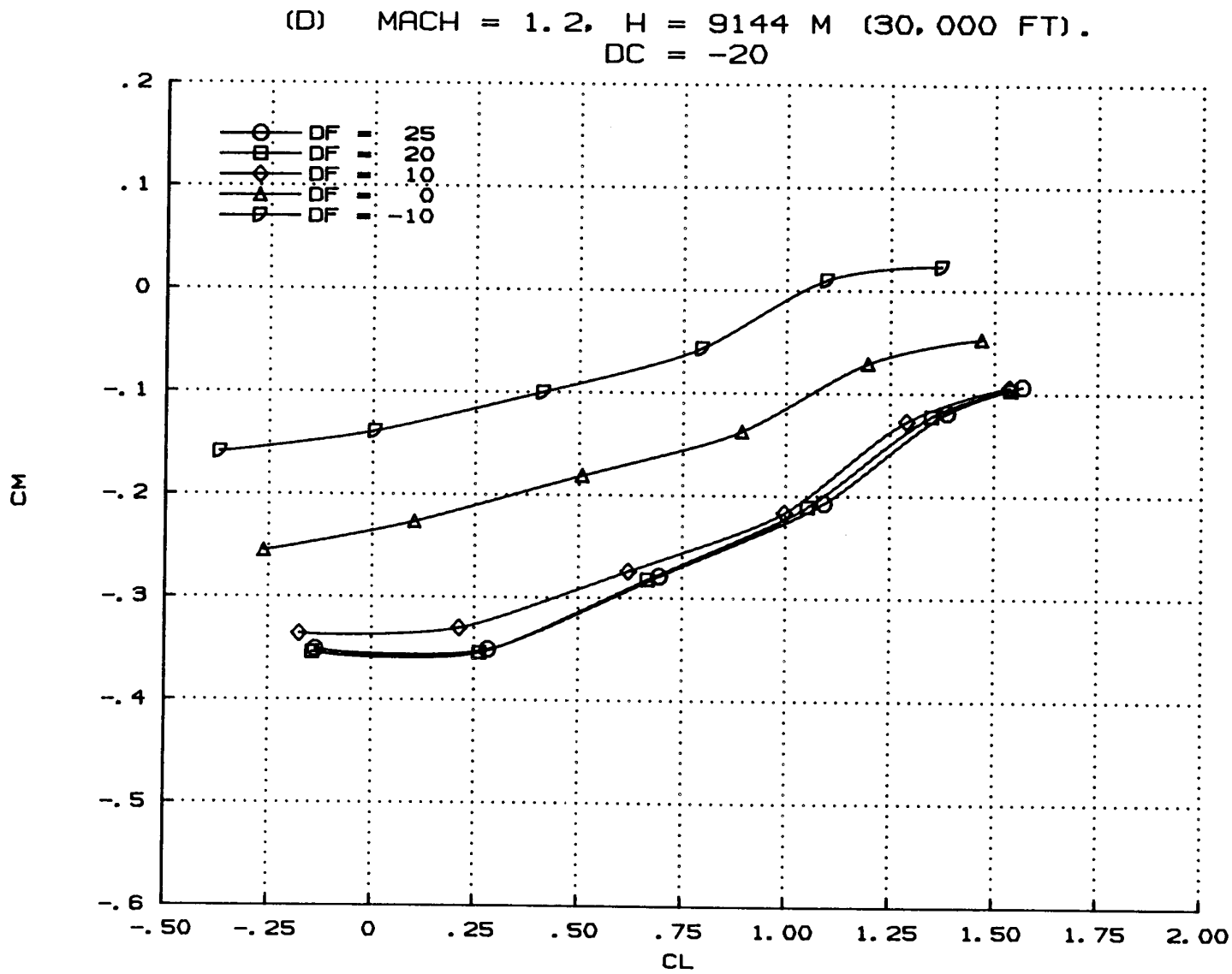

FIGURE 7. CM AS A FUNCTION OF CL. FLEXIBLE, VARYING DF.

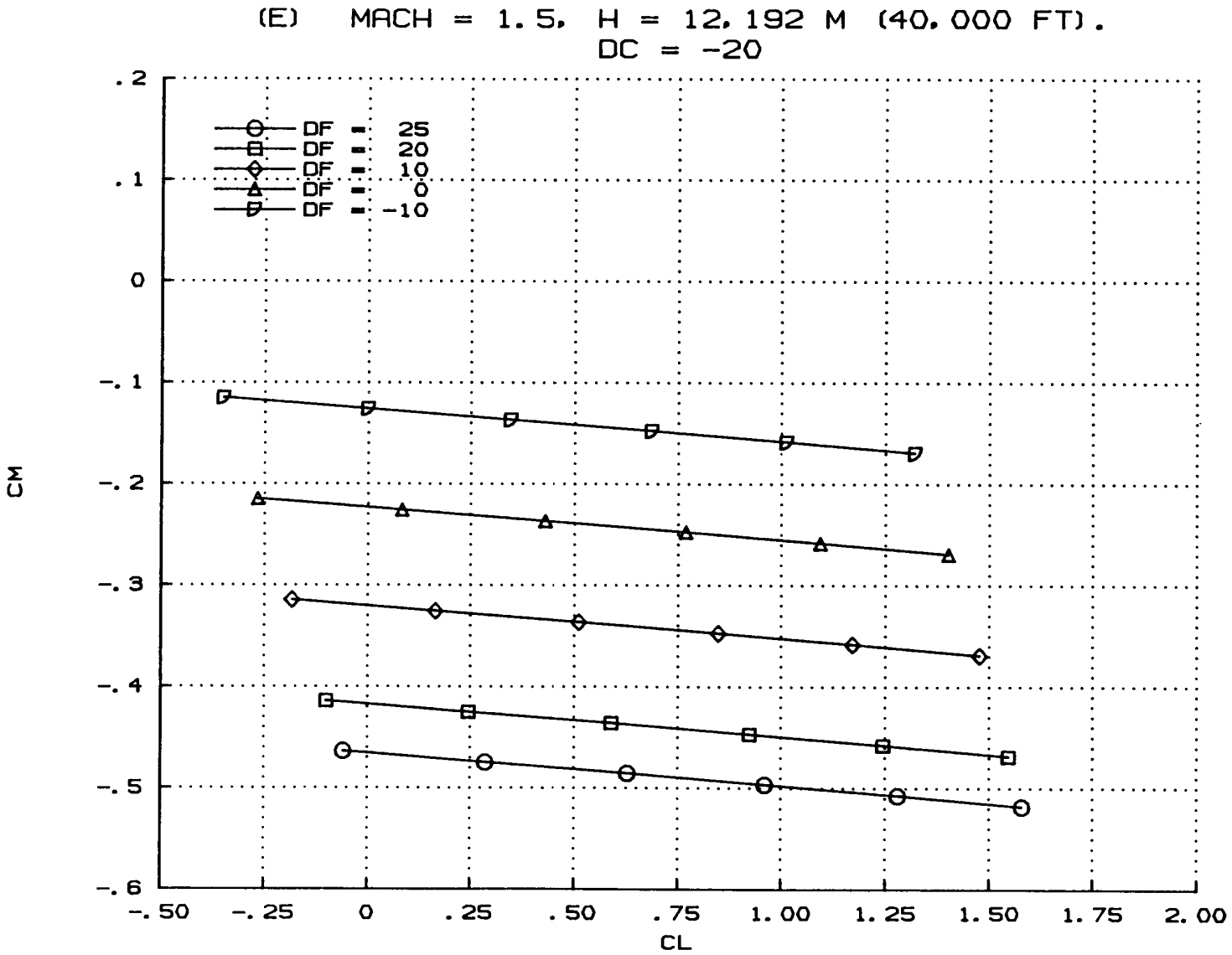

FIGURE 7. CM AS A FUNCTION OF CL. FLEXIBLE, VARYING DF.

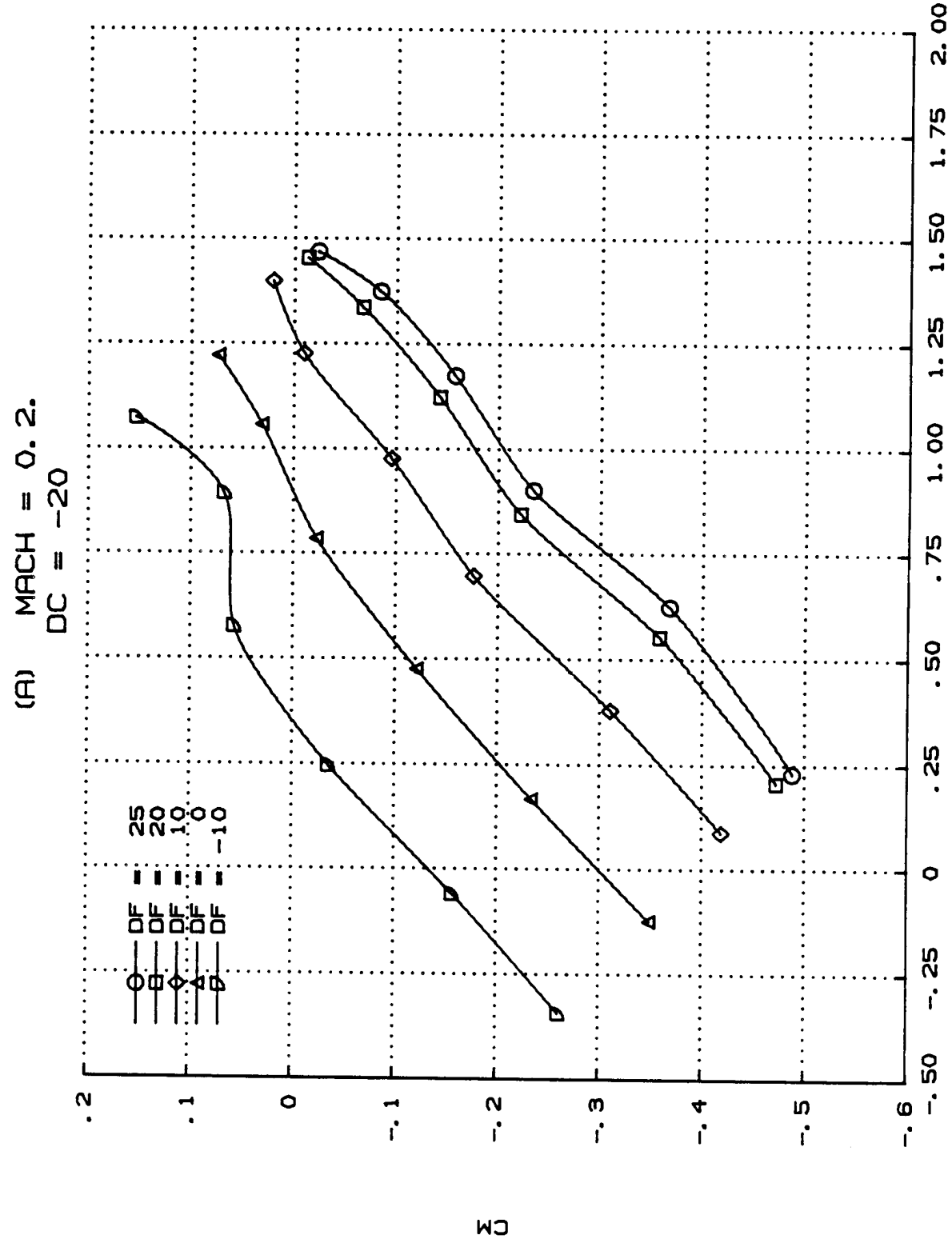

FIGURE 8. CM AS A FUNCTION OF CL. RIGID. VARYING DF.

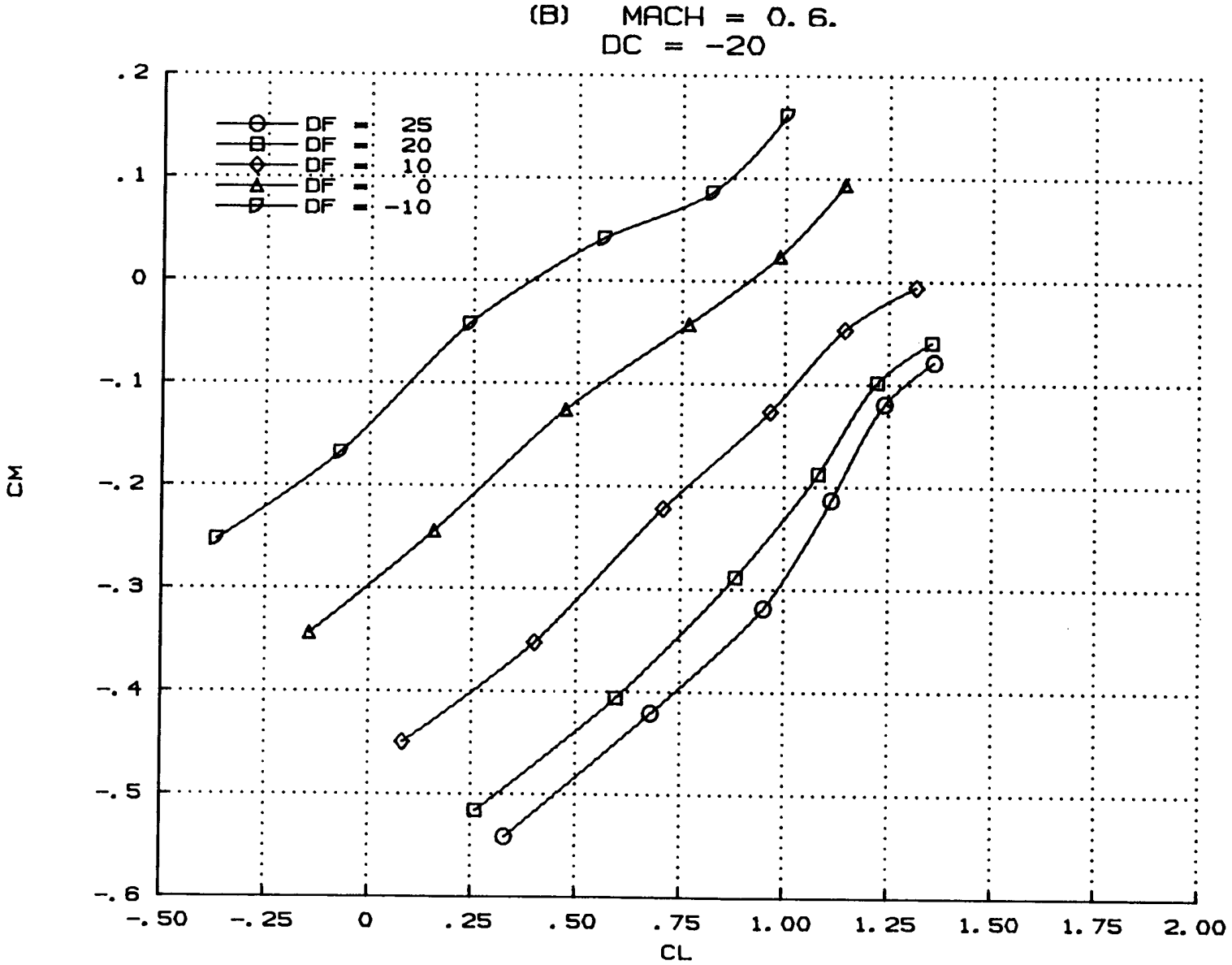

FIGURE 8. CM AS A FUNCTION OF CL. RIGID. VARYING DF.

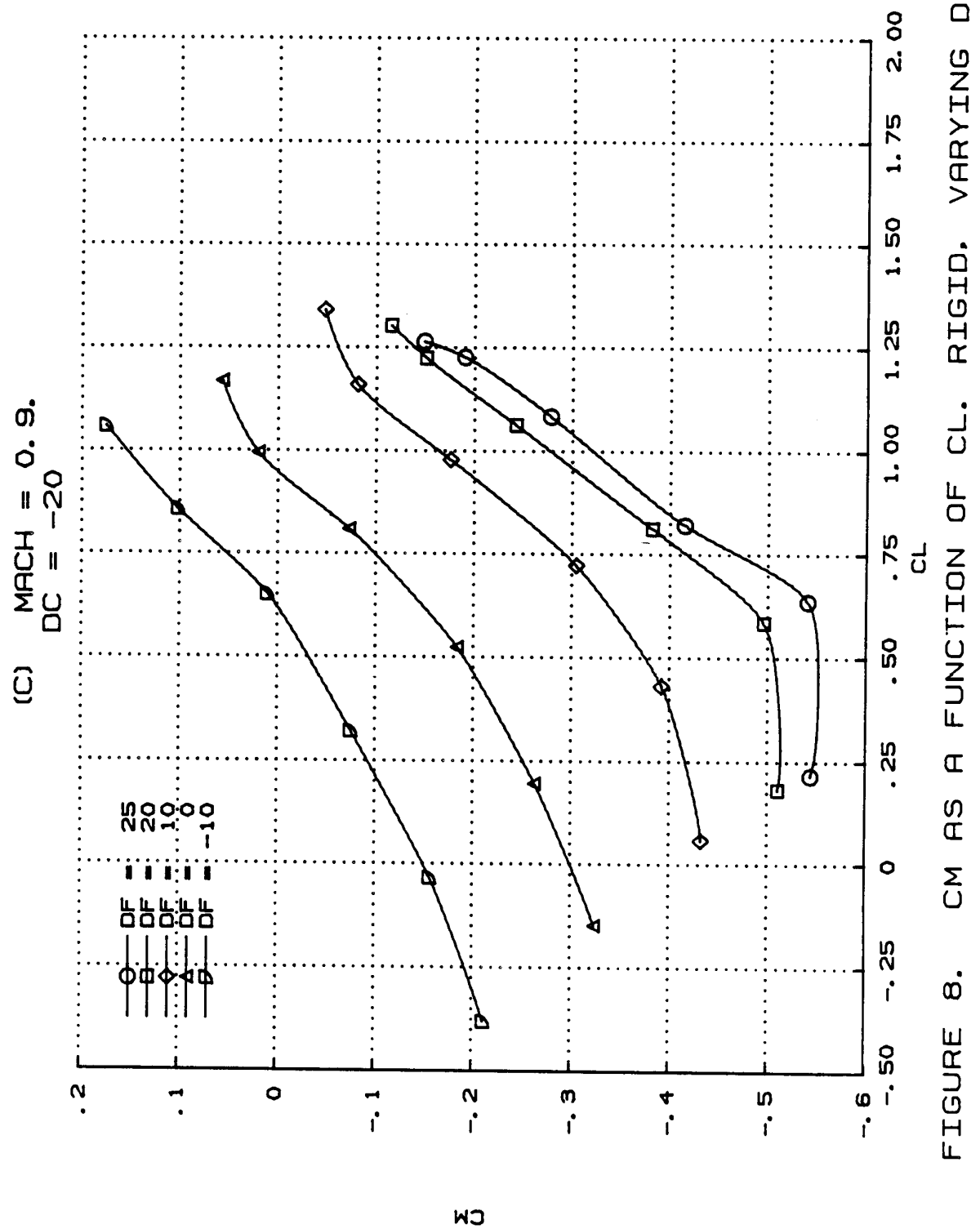

FIGURE 8. CM AS A FUNCTION OF CL. RIGID. VARYING DF.

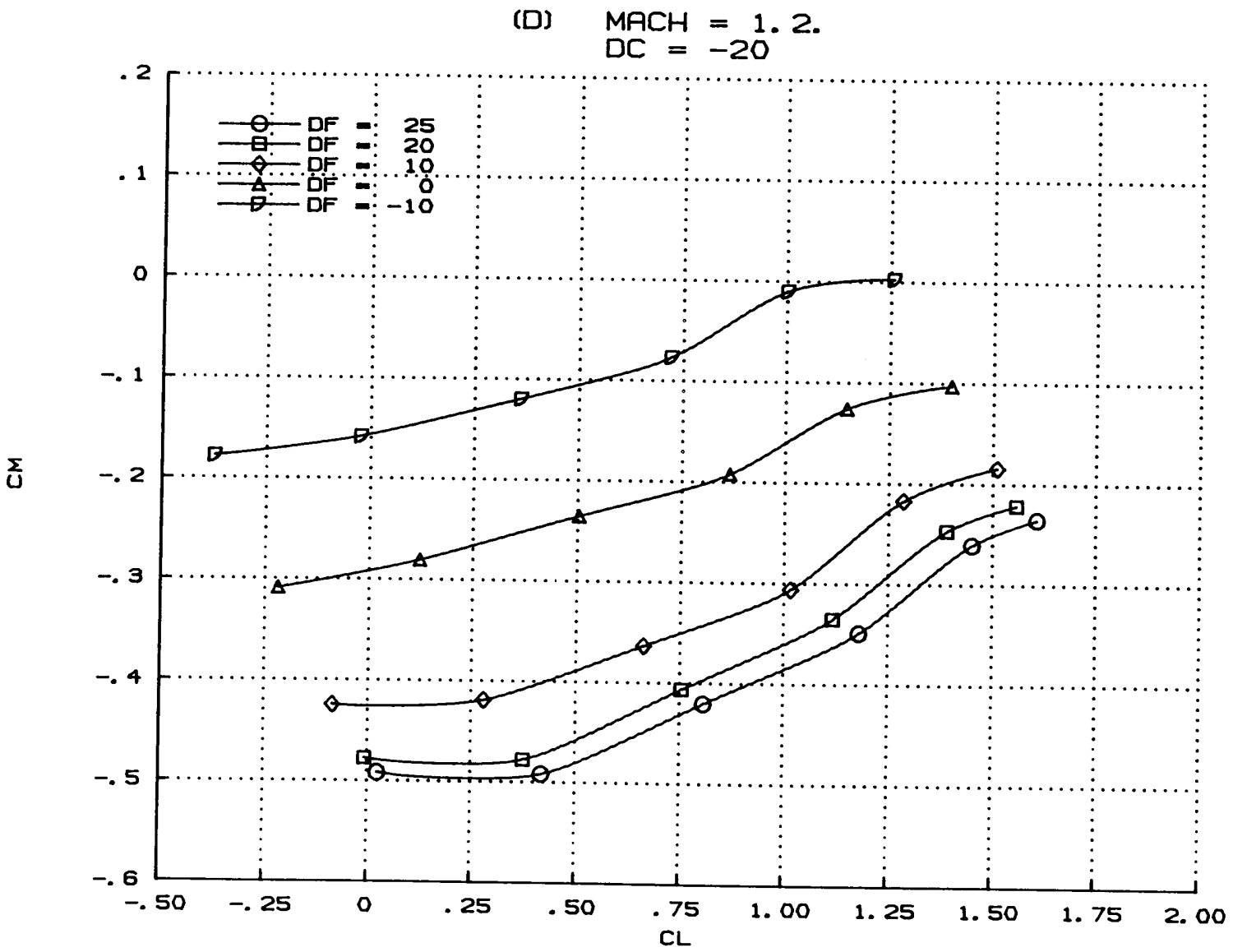

FIGURE 8. CM AS A FUNCTION OF CL. RIGID. VARYING DF.

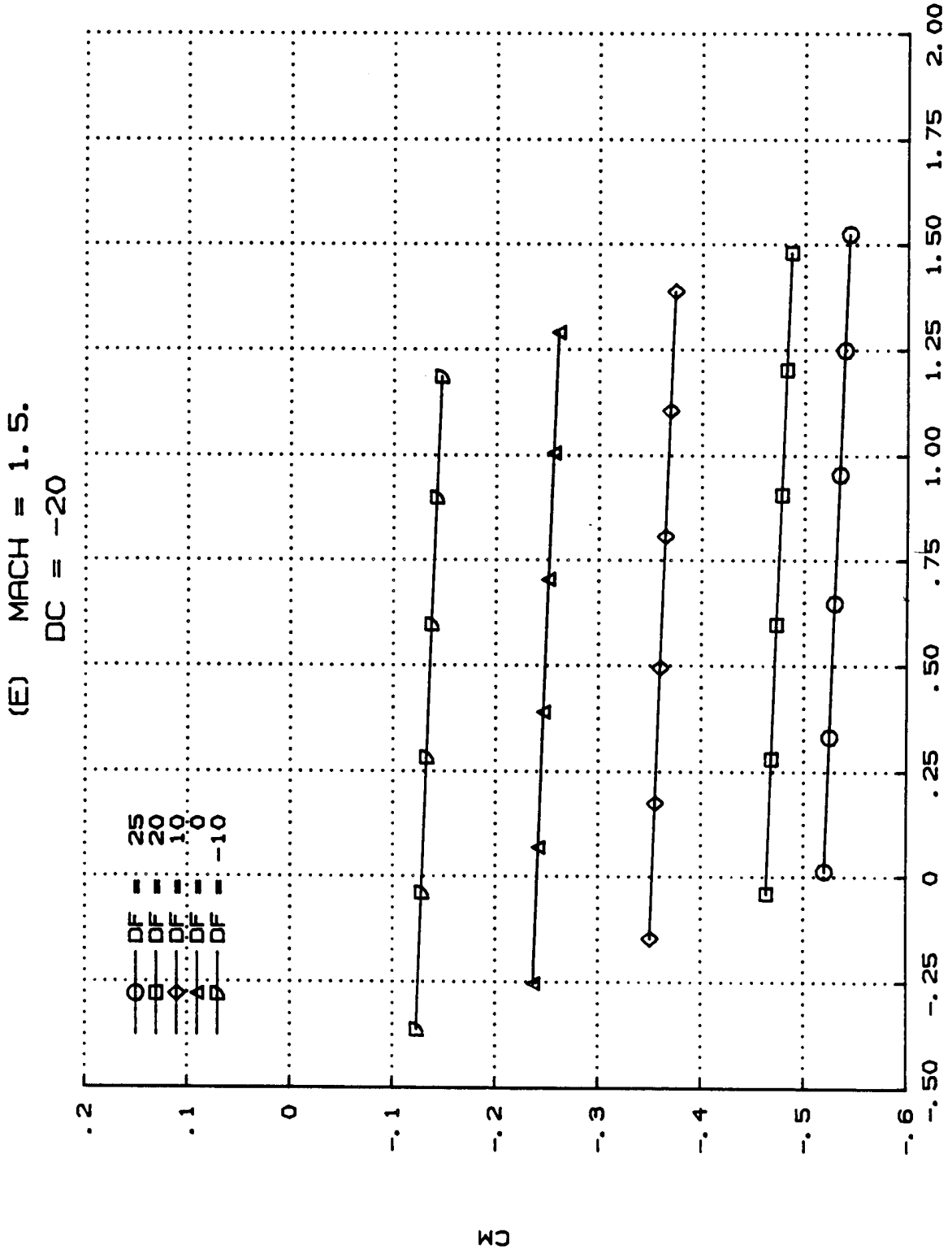

FIGURE 8. CM AS A FUNCTION OF CL. RIGID, VARYING DF.

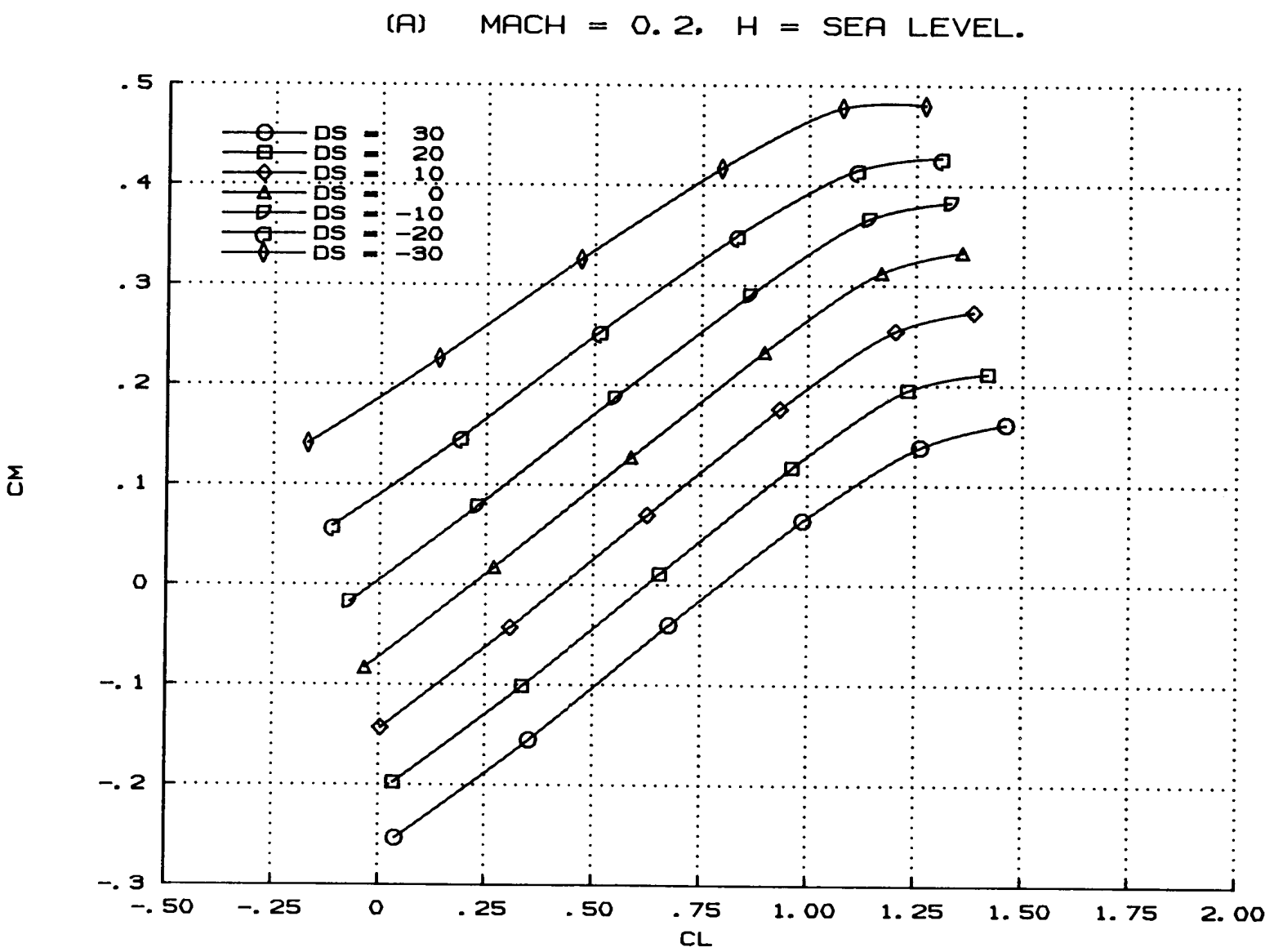

FIGURE 9. CM AS A FUNCTION OF CL. FLEXIBLE. VARYING DS.

(B) MACH = 0.6, H = 4572 M (15,000 FT).

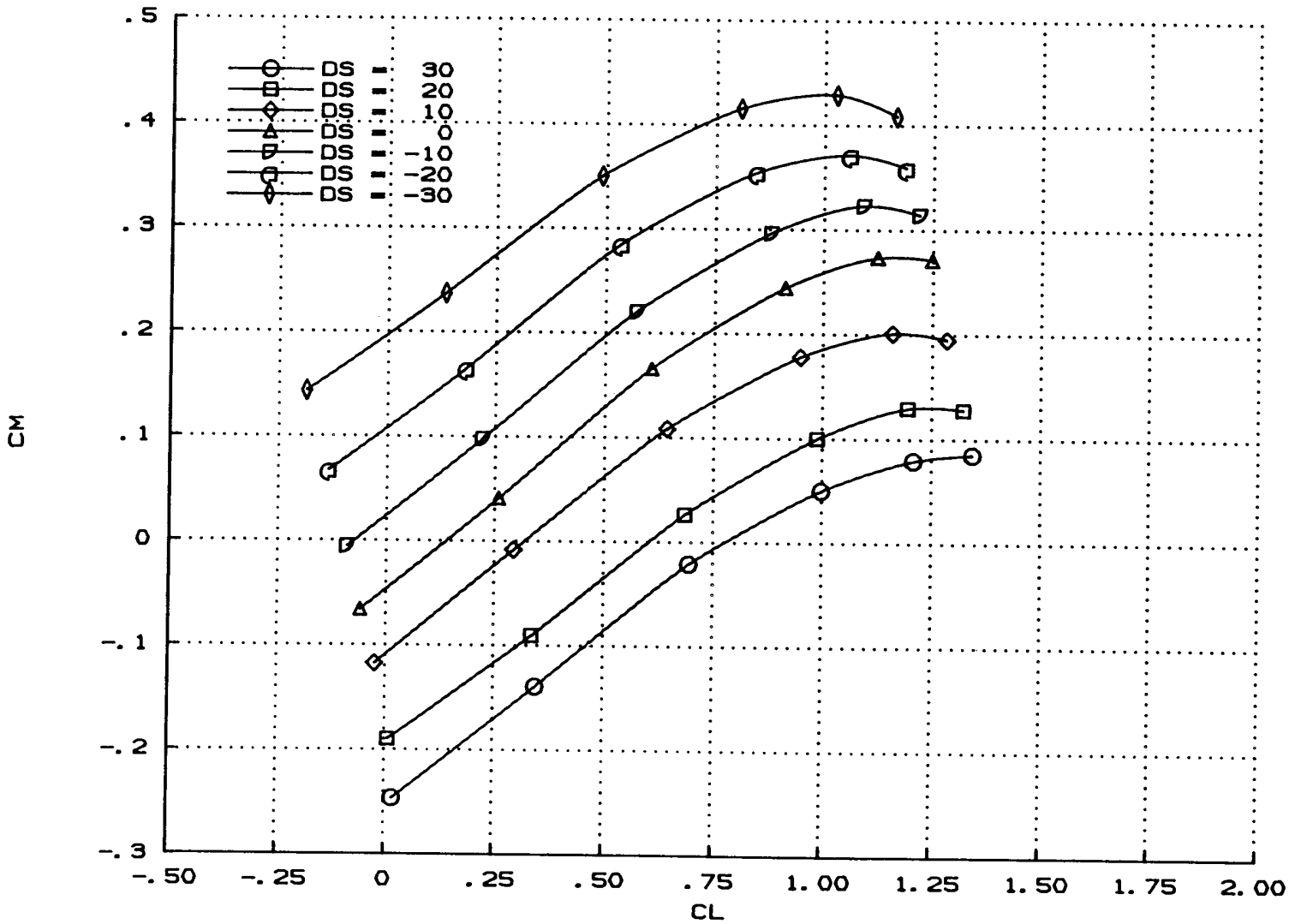

FIGURE 9. CM AS A FUNCTION OF CL. FLEXIBLE, VARYING DS.

(C) MACH = 0.9, H = 9144 M (30,000 FT).

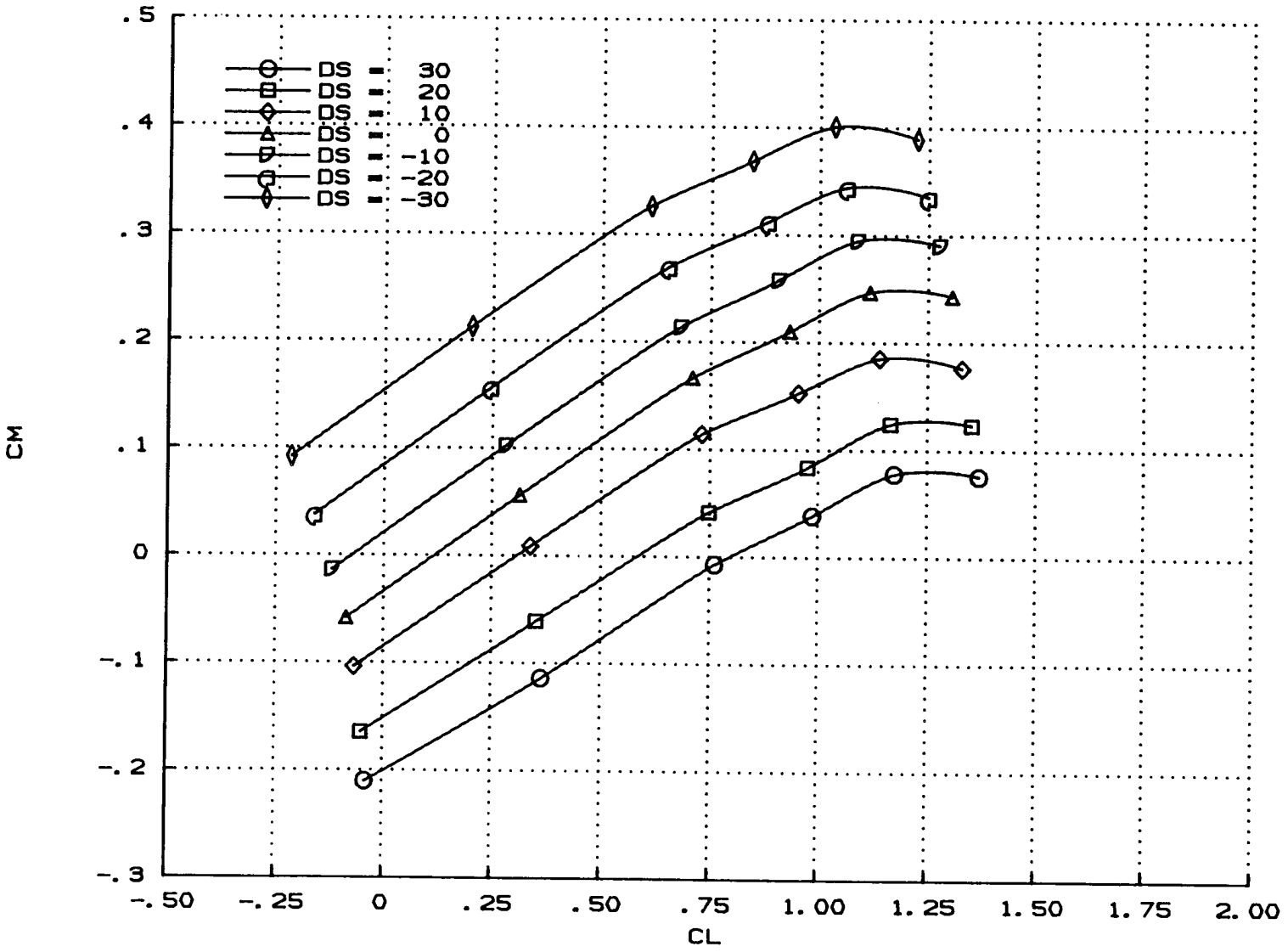

FIGURE 9. CM AS A FUNCTION OF CL. FLEXIBLE, VARYING DS.

(D) MACH = 1.2, H = 9144 M (30,000 FT).

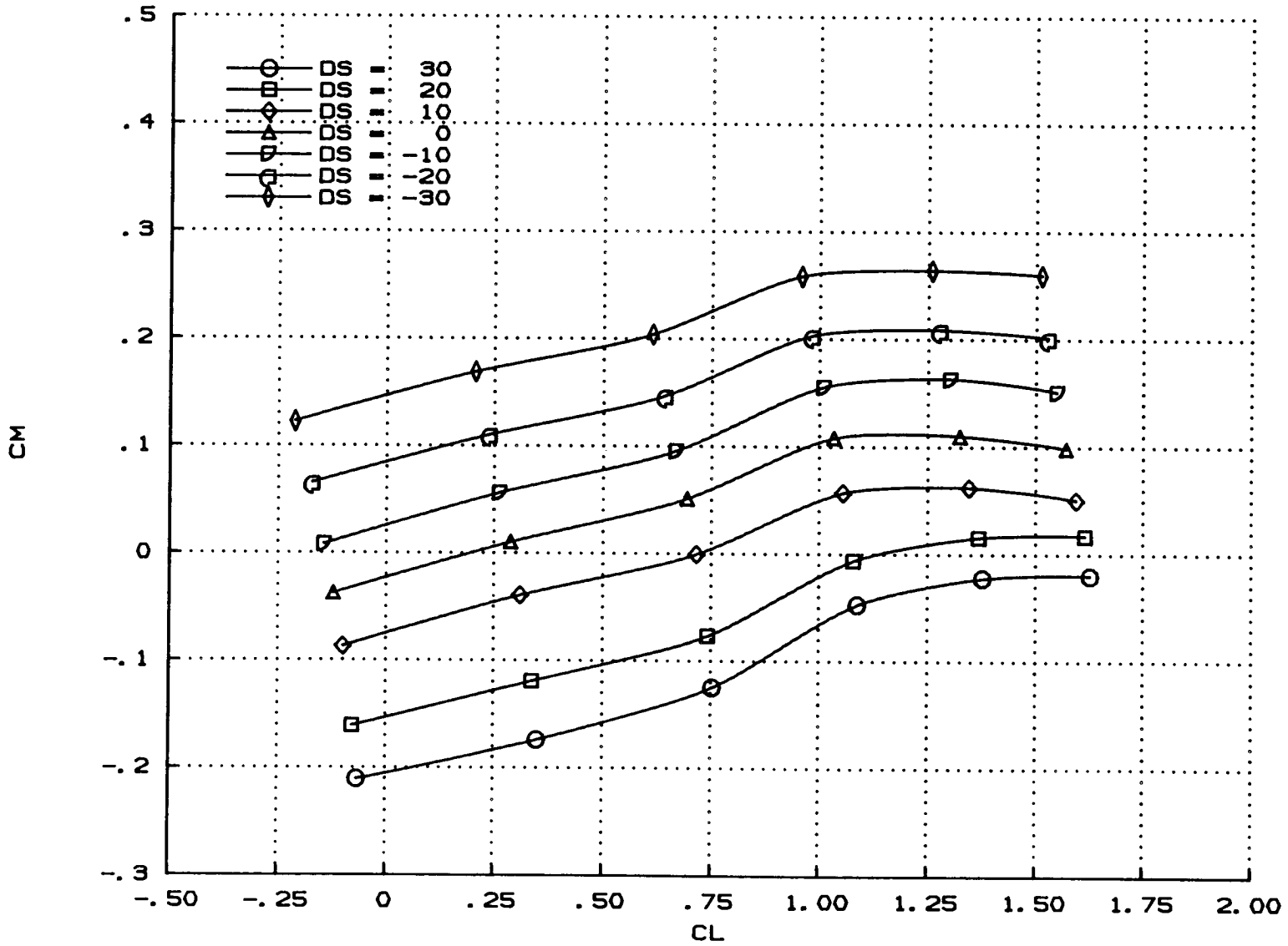

FIGURE 9. CM AS A FUNCTION OF CL. FLEXIBLE. VARYING DS.

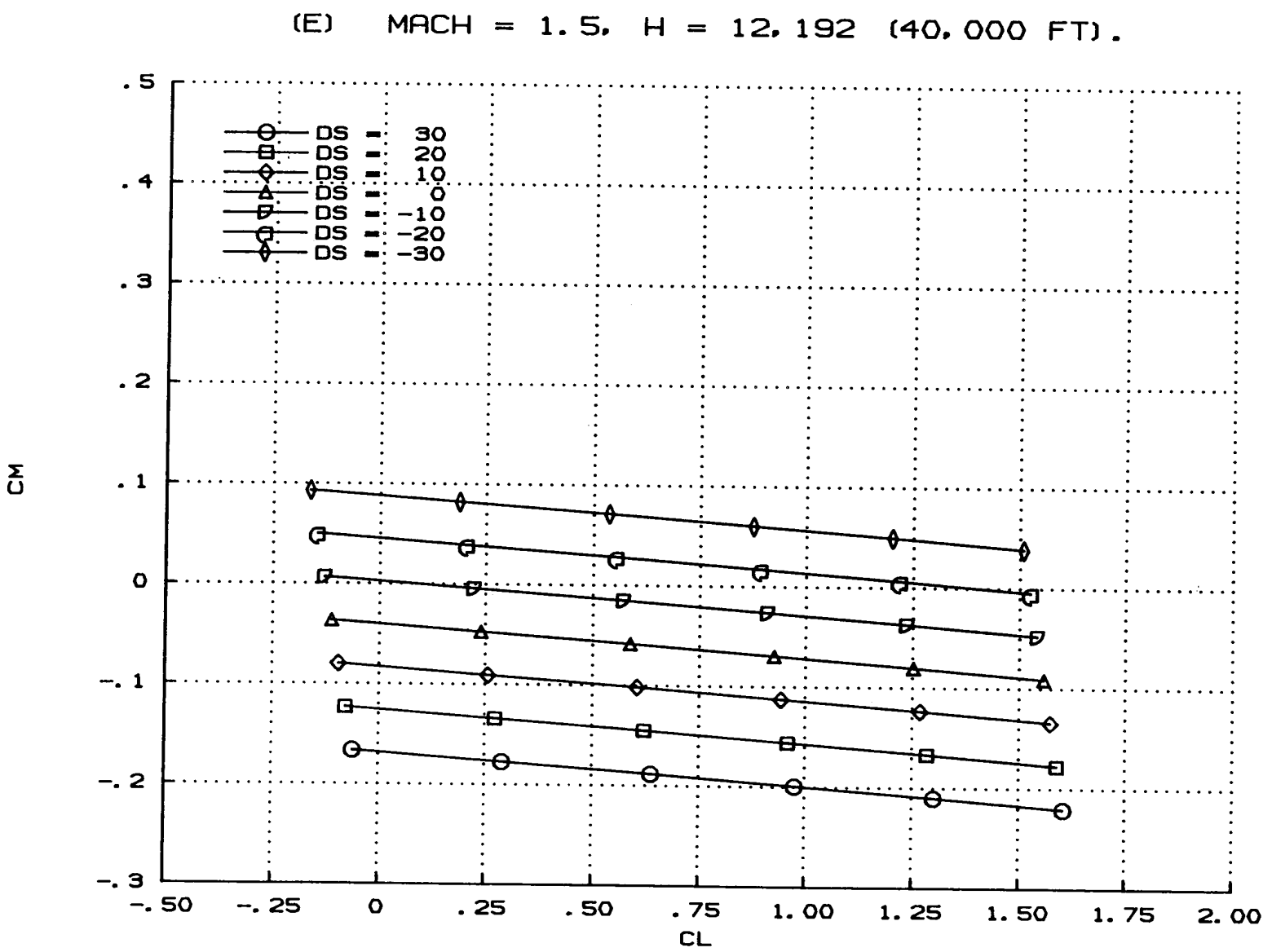

FIGURE 9. CM AS A FUNCTION OF CL. FLEXIBLE, VARYING DS.

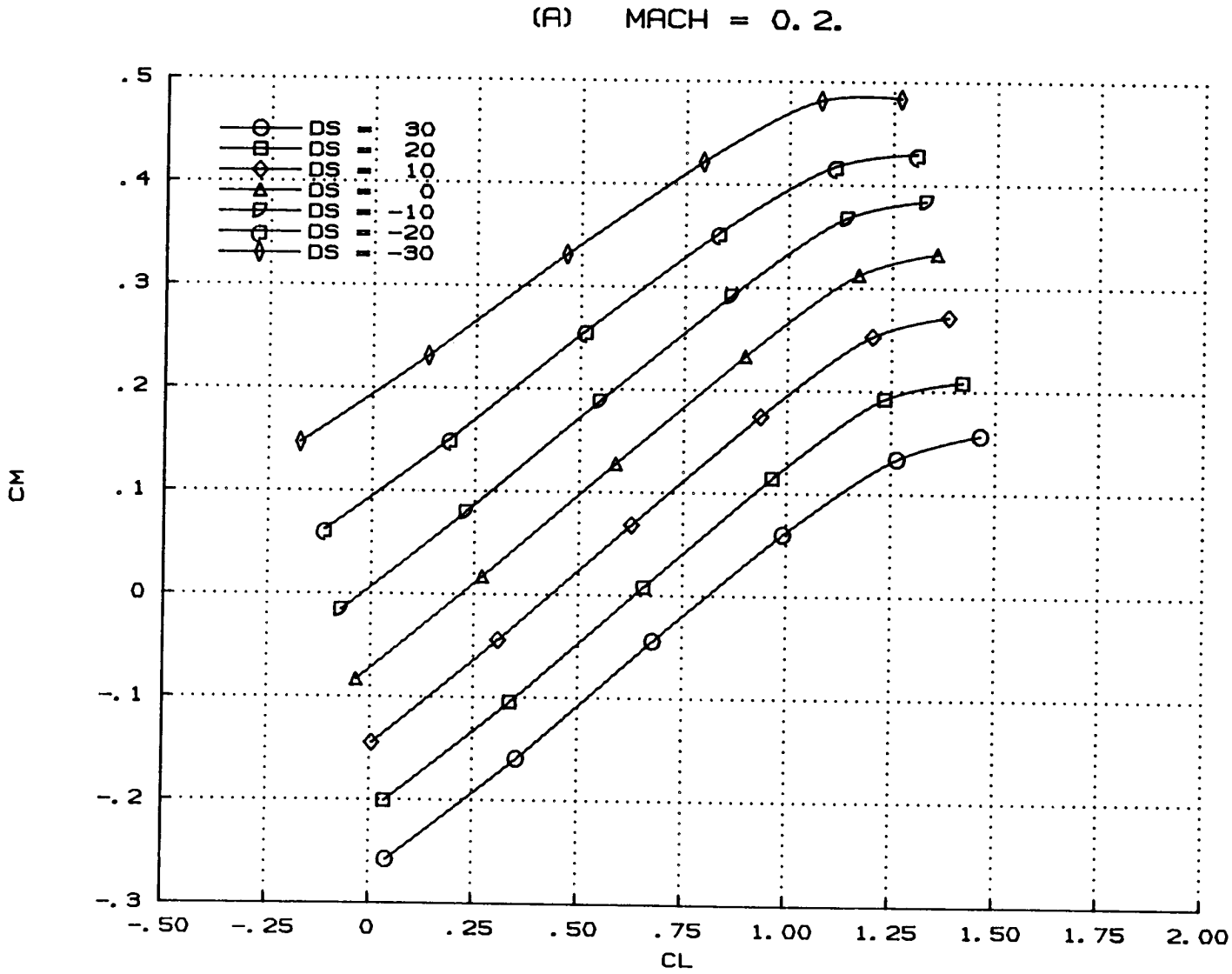

FIGURE 10. CM AS A FUNCTION OF CL. RIGID. VARYING DS.

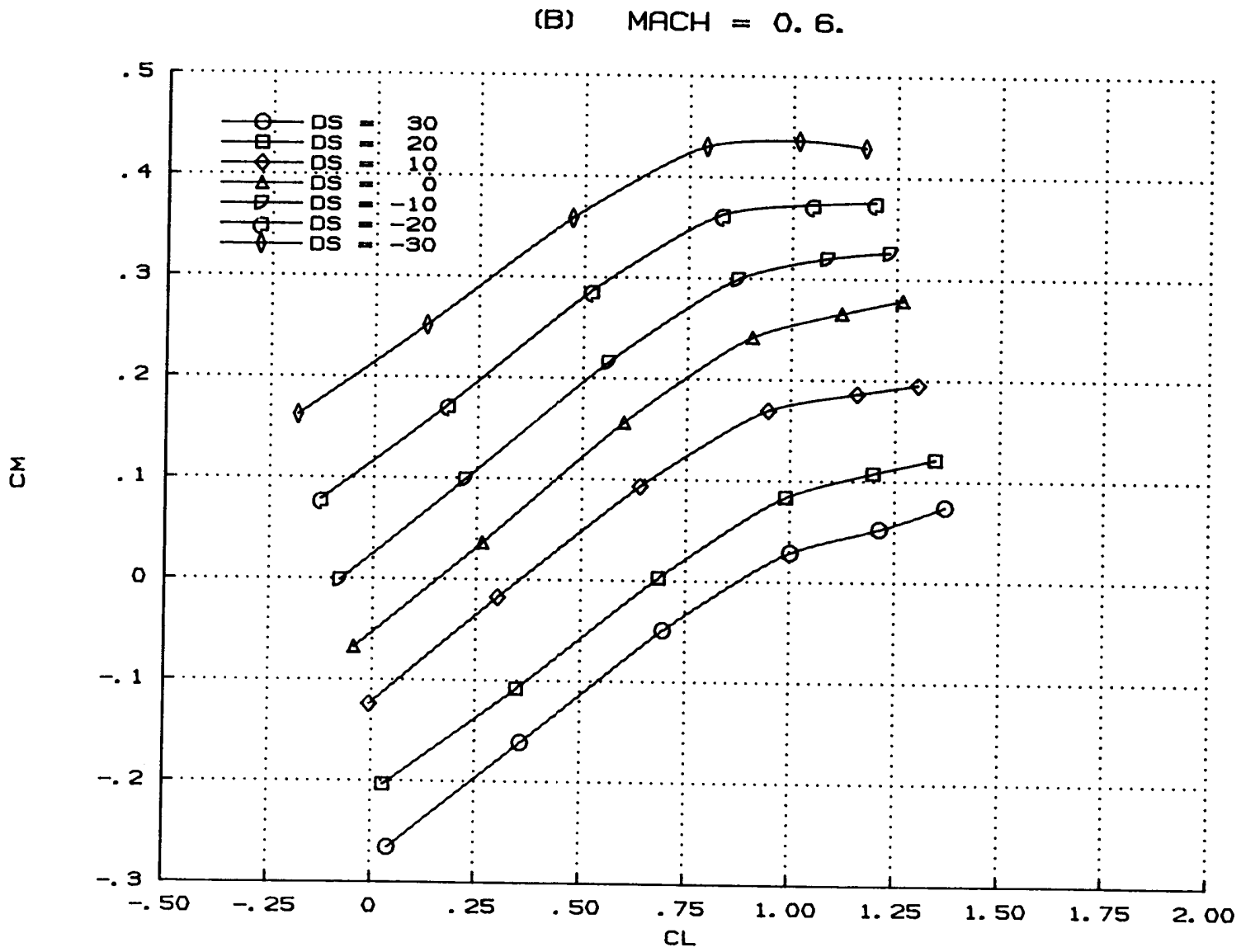

FIGURE 10. CM AS A FUNCTION OF CL. RIGID, VARYING DS.

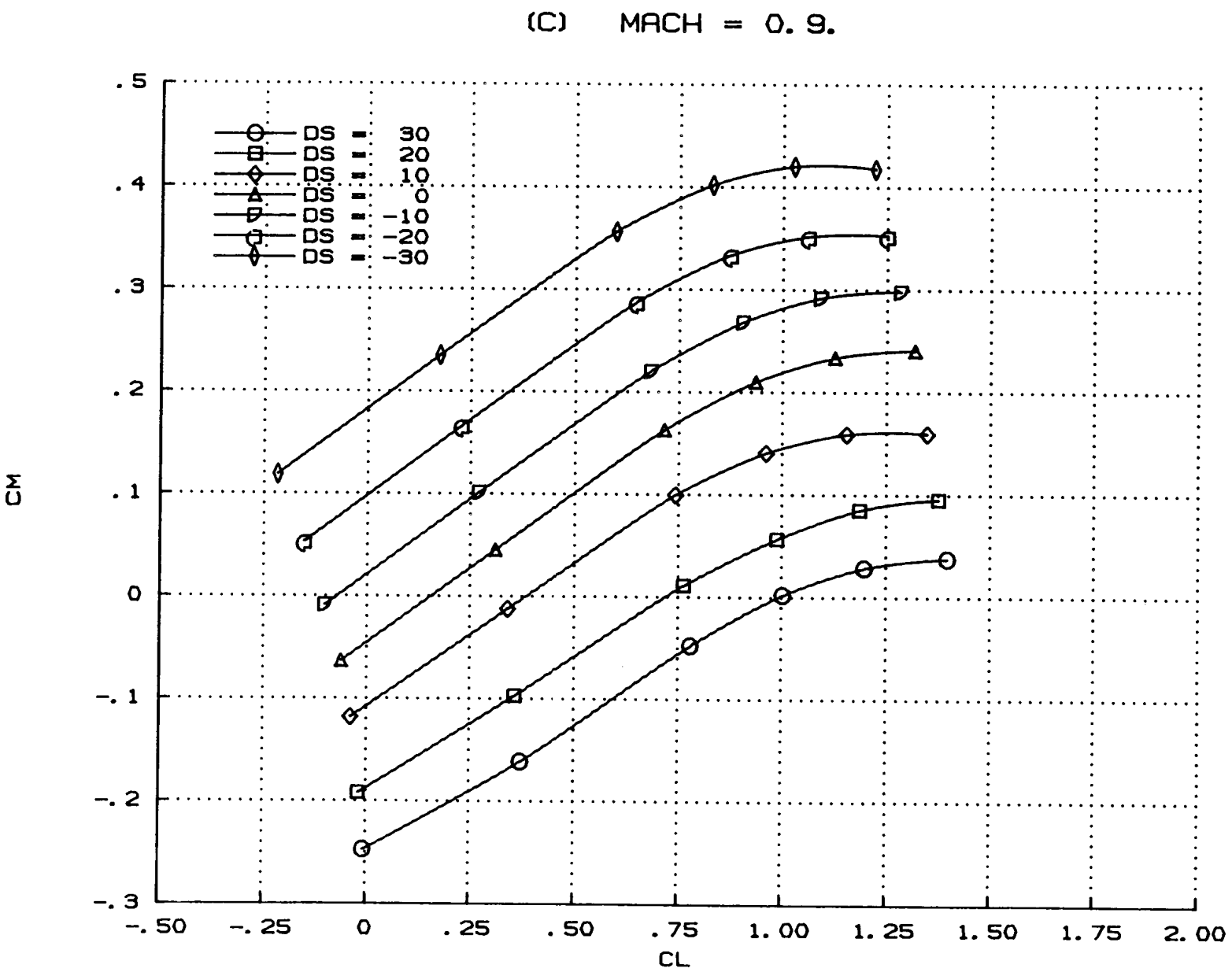

FIGURE 10. CM AS A FUNCTION OF CL. RIGID, VARYING DS.

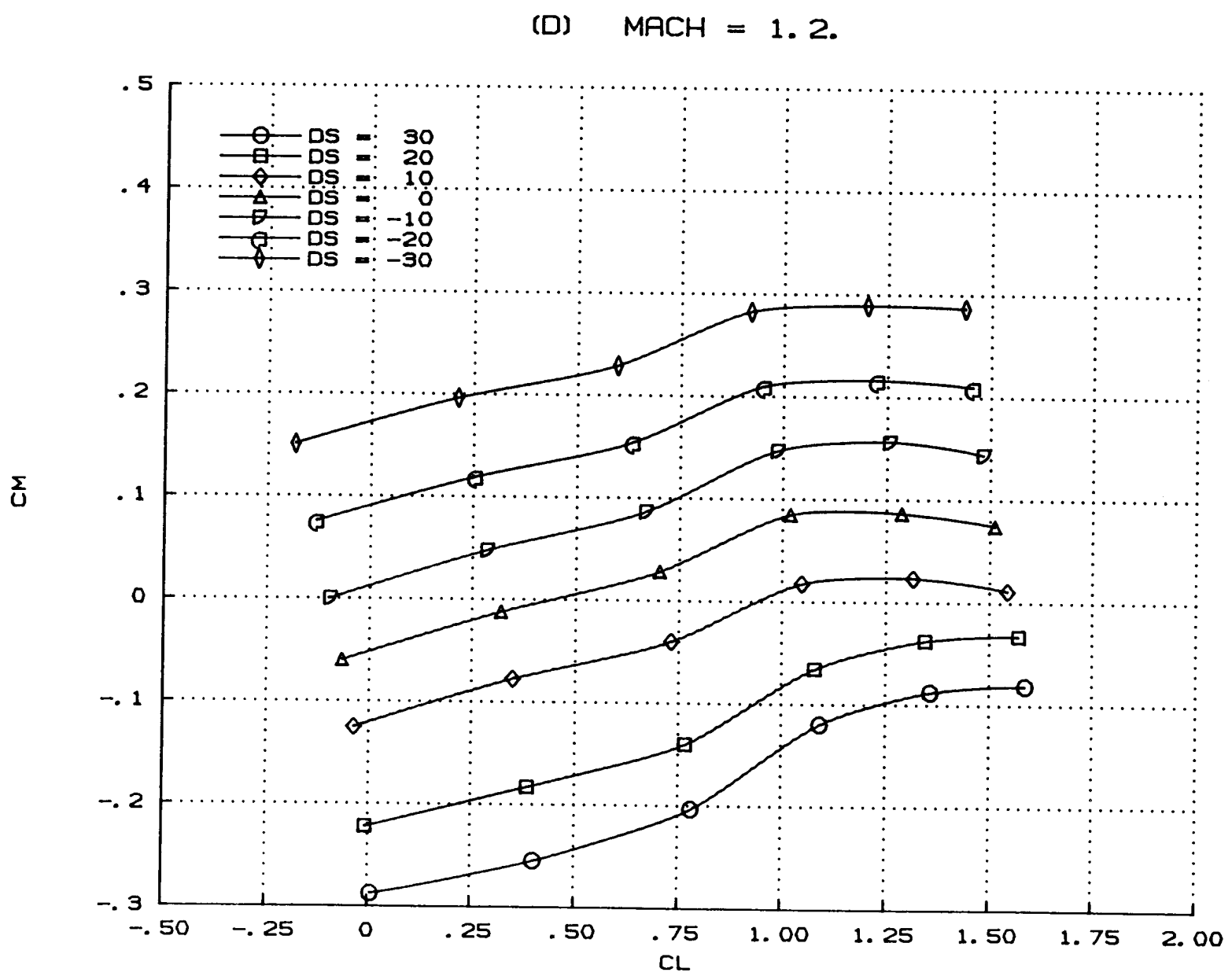

FIGURE 10. CM AS A FUNCTION OF CL. RIGID. VARYING DS.

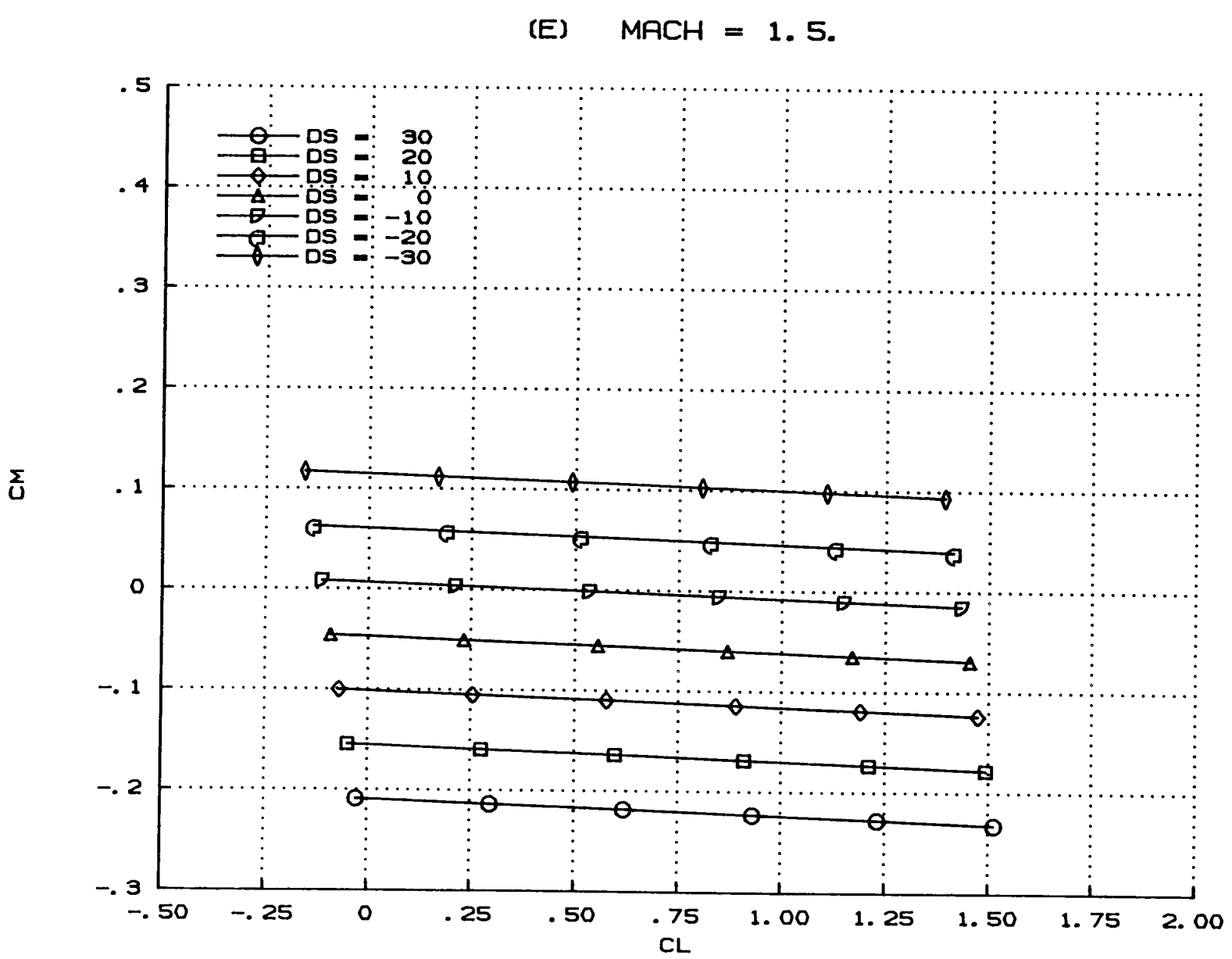

FIGURE 10. CM AS A FUNCTION OF CL. RIGID, VARYING DS.

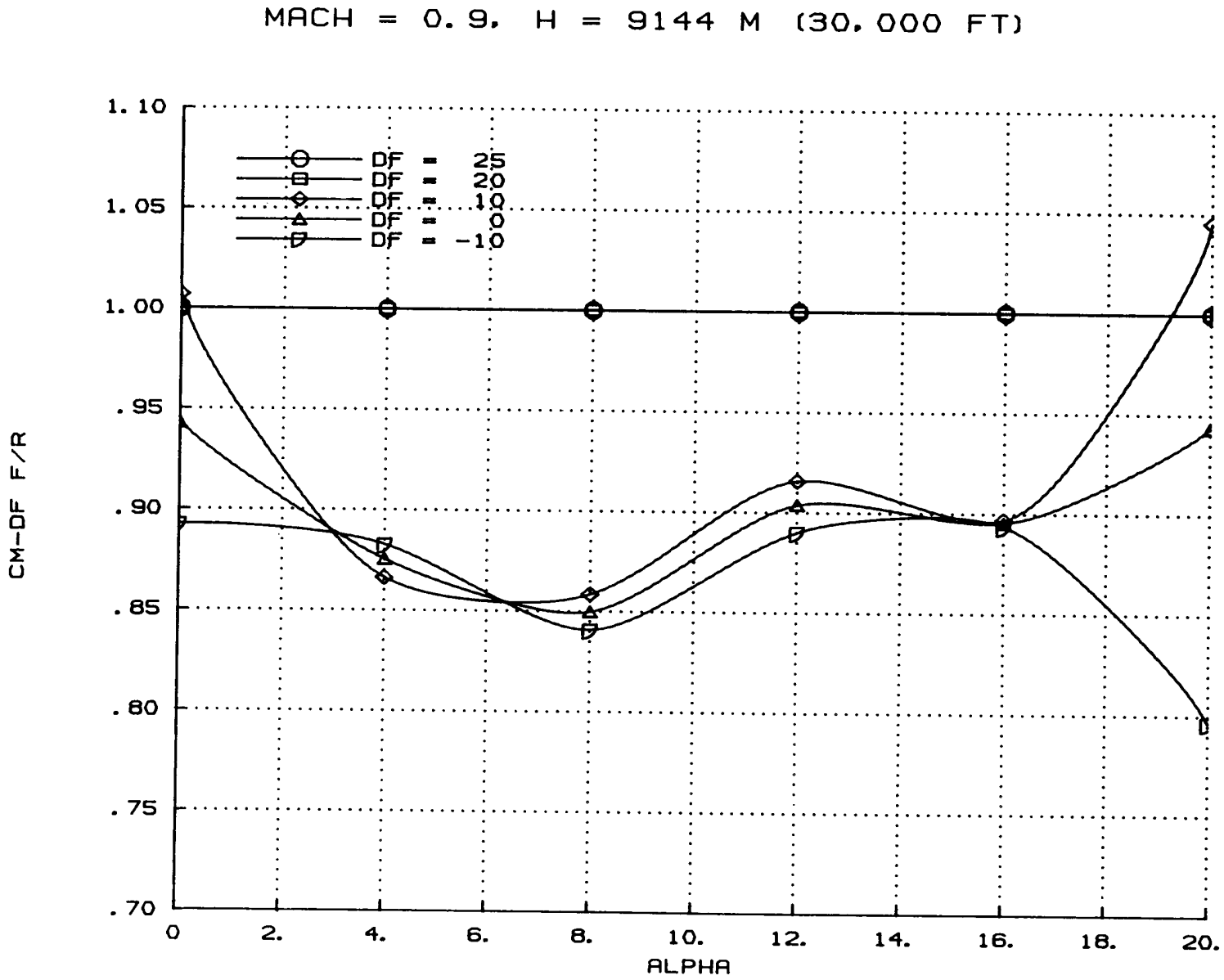

FIGURE 11. WING FLAP PITCH CONTROL FLEXIBLE/RIGID RATIO

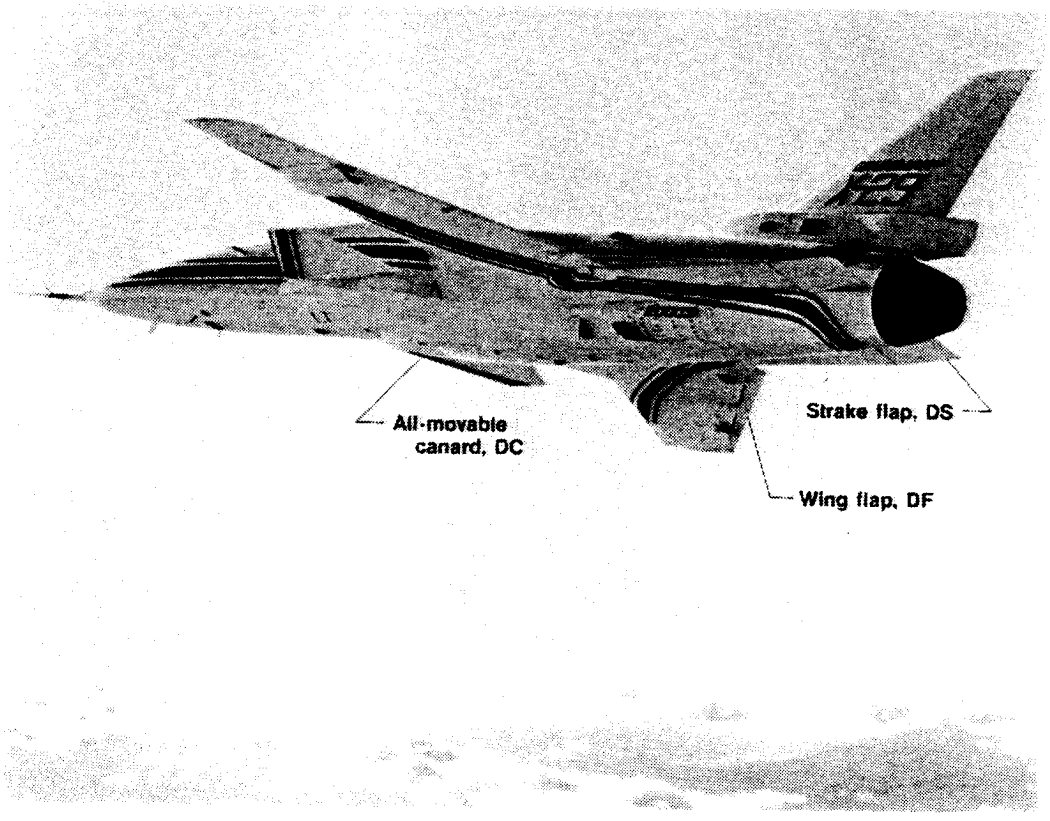

Figure 12. X-29A aircraft.

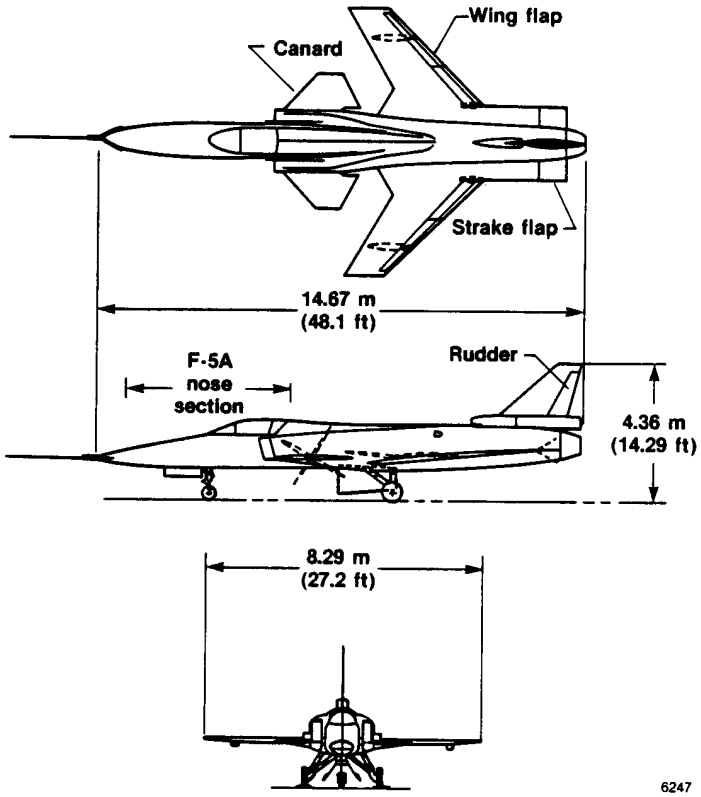

Figure 13. General configuration of X-29A aircraft.

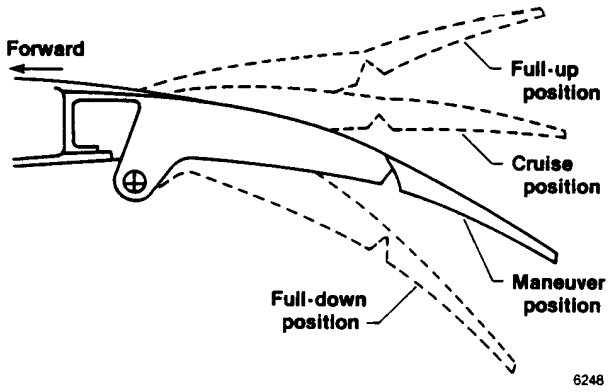

[redacted] *Full-span flap geometry.*

1. Report No.	2. Government Accession No.	3. Recipient's Catalog No.
NASA TM-88284		

4. Title and Subtitle	5. Report Date
Predicted Pitching Moment Characteristics of X-29A Aircraft	March 1987
	6. Performing Organization Code
7. Author(s)	8. Performing Organization Report No.
Gerald D. Budd	H-1398
9. Performing Organization Name and Address	10. Work Unit No.
NASA Ames Research Center Dryden Flight Research Facility P.O. Box 273 Edwards, CA 93523-5000	RTOP 533-02-51
	11. Contract or Grant No.
12. Sponsoring Agency Name and Address	13. Type of Report and Period Covered
National Aeronautics and Space Administration Washington, DC 20546	Technical Memorandum
	14. Sponsoring Agency Code

15. Supplementary Notes

16. Abstract

The predicted pitching moment characteristics of the X-29A aircraft are presented for angles of attack from 0 to 20° and Mach numbers of 0.2, 0.6, 0.9, 1.2, and 1.5 for altitudes of sea level, 4572 m (15,000 ft), 9144 m (30,000 ft), and 12,192 m (40,000 ft). These data are for both rigid and flexible aircraft and for the full range of control-surface positions. The characteristics were extracted from a nonlinear, symmetric, flexibilized wind tunnel data base.

17. Key Words (Suggested by Author(s))	18. Distribution Statement
Close-coupled canard Forward-swept wing Pitching moment characteristics X-29 aircraft	Subject category 02

19. Security Classif. (of this report)	20. Security Classif. (of this page)	21. No. of Pages	22. Price*
Unclassified	Unclassified	64	A04